The chromatin-remodeling enzyme Smarca5 regulates erythrocyte aggregation via Keap1-Nrf2 signaling

Yanyan Ding[1, 2, 3#], Yuzhe Li[4, 6#], Qiangfeng Cliff Zhang[4, 5], and Feng Liu[1, 2, 3*]

[1]State Key Laboratory of Membrane Biology, Institute of Zoology, Chinese Academy of Sciences, Beijing 100101, China;

[2] Institute for Stem Cell and Regeneration, Chinese Academy of Sciences, 100101 Beijing, China;

[3]University of Chinese Academy of Sciences, Beijing 100049, China;

[4]MOE Key Laboratory of Bioinformatics, Beijing Advanced Innovation Center for Structural Biology & Frontier Research Center for Biological Structure, Center for Synthetic and Systems Biology, School of Life Sciences, Tsinghua University, Beijing, China 100084;

[5]Tsinghua-Peking Center for Life Sciences, Beijing, China 100084;

[6]Academy for Advanced Interdisciplinary Studies, Peking University, Beijing, China 100871

[#] These authors contributed equally to this work.

[*] Corresponding author

Prof. Feng Liu, PhD

State Key Laboratory of Membrane Biology

Institute of Zoology, Chinese Academy of Sciences

Beijing, 100101, China

Email: liuf@ioz.ac.cn

Tel.: +86 (10) 64807307 Fax: +86 (10) 64807313

Abstract

Although thrombosis has been extensively studied using various animal models, however, our understanding of the underlying mechanism remains elusive. Here, using zebrafish model, we demonstrated that *smarca5*-deficient red blood cells (RBCs) formed blood clots in the caudal vein plexus that mimics venous thrombosis. We further used the anti-thrombosis drugs to treat *smarca5*^{zko1049a} embryos and found that a thrombin inhibitor, argatroban, partially prevented blood clot formation in *smarca5*^{zko1049a}. To explore the regulatory mechanism of *smarca5* in RBC homeostasis, we profiled the chromatin accessibility landscape and transcriptome features in RBCs from *smarca5*^{zko1049a} and their siblings and found that both the chromatin accessibility at the *keap1a* promoter and expression of *keap1a* were decreased. Keap1 is a suppressor protein of Nrf2, which is a major regulator of oxidative responses. We further identified that the expression of *hmox1a*, a downstream target of Keap1-Nrf2 signaling pathway, was markedly increased upon *smarca5* deletion. Importantly, overexpression of *keap1a* or knockdown of *hmox1a* partially rescued the blood clot formation, suggesting that the disrupted Keap1-Nrf2 signaling is responsible for the venous thrombosis-like phenotypes in *smarca5* mutants. Together, our study using zebrafish *smarca5* mutants not only characterizes a novel role for *smarca5* in blood clot formation, but also provides a new venous thrombosis animal model to support drug screening and pre-clinical therapeutic assessments to treat thrombosis.

Introduction

The erythrocytes, or red blood cells (RBCs), are highly differentiated cells produced during erythropoiesis. Mature RBCs are characterized for their abundance of hemoglobin, which can deliver oxygen to surrounding tissues. Importantly, the flexible structure of RBCs makes it capable of traveling through all blood vessels including capillaries by deformation (Rodriguez-Garcia et al., 2016). On the benefit of accumulated hemoglobin and the deformation ability, RBCs are essential for organism development by facilitating tissue oxygen delivery and transporting carbon dioxide into the respiration tissues. Moreover, RBCs participate in the maintenance of thrombosis and hemostasis (Weisel & Litvinov, 2019).

Epigenetic regulation of RBC-related genes is fundamental for normal development and maintenance of RBCs (Hewitt, Sanalkumar, Johnson, Keles, & Bresnick, 2014). In this process, the regulation of chromatin accessibility is a prerequisite for gene transcription and is regulated by chromatin remodelers. For instance, Brg1 could regulate α- and β-globin gene transcription in primitive erythrocytes in mice (Bultman, Gebuhr, & Magnuson, 2005; Griffin, Brennan, & Magnuson, 2008). The nucleosome remodeling and histone deacetylase (NuRD) is identified to activate human adult-type globin gene expression (Miccio & Blobel, 2010).

Disorder of the gene regulation in RBCs will lead to cellular defects, thereby causing multiple diseases, such as hemoglobinopathy-induced anemia, RBC lysis-induced hemolytic anemia and thrombosis (Kato et al., 2018; Roumenina, Rayes, Lacroix-Desmazes, & Dimitrov, 2016; Weisel & Litvinov, 2019). Among them, thrombosis is a leading cause of death worldwide (Wendelboe & Raskob, 2016). In contrast to arterial thrombi, which are rich in platelets, the venous thrombi are enriched in fibrin and RBCs (Mackman, 2008; Mackman, Bergmeier, Stouffer, & Weitz, 2020). Moreover, venous thrombi can break off, travel and lodge in the lung, thereby causing pulmonary embolism (Wolberg et al., 2015).

Currently, the ligature-based inferior vena cava models, free radical thrombosis models and genetic knockout models are widely used in mice to study deep vein thrombosis (Diaz et al., 2019; Grover & Mackman, 2019). These disease models are generated mainly through disrupting blood flow, endothelium and blood coagulability. Taking advantage of the conserved hemostatic system and the transparency of embryos, zebrafish has been also used to generate thrombosis models. For instance, phenylhydrazine-treated zebrafish develop severe thrombosis in the caudal vein (Zhu et

al., 2016). Mechanistically, phenylhydrazine causes externalization of phosphatidylserine on plasma of RBC membrane and generates oxidative radicals, thereafter, resulting in the thrombosis formation. These studies in animal models shed light on the understanding and treatment of vaso-occlusion phenotype in patients with RBC defects. However, the detailed kinetics and underlying mechanism of thrombosis formation in these models are not fully explored.

In our previous study, genetic deletion of an epigenetic regulator-*smarca5* (*smarca5*^{zko1049a}) resulted in abnormal chromatin accessibility, and we observed disruption of hematopoietic transcription factor binding in the genome, finally leading to defects in fetal hematopoietic stem and progenitor cells (HSPCs) (Ding et al., 2021). However, whether the other hematopoietic cell types are regulated by *smarca5* is unknown. Here, we develop a new zebrafish thrombosis model with a deletion of *smarca5*, loss of which leads to the formation of blood clots in the caudal vein plexus (CVP). We further present how exactly the change in the subcellular structure of *smarca5*-deficient RBCs occurred using transmission electron microscopy (TEM), and uncovered the disintegration of cristae in mitochondria in RBCs. To explore the regulatory mechanism of *smarca5* in RBC homeostasis, we profiled the chromatin accessibility landscape and transcriptome features by performing Assay for Transposase-Accessible Chromatin with high-throughput sequencing (ATAC-seq) and RNA sequencing (RNA-seq) analyses in RBCs from *smarca5*^{zko1049a} and their siblings. Mechanistically, loss of *smarca5* led to the decreased chromatin accessibility at *keap1a* promoter and thus decreased transcriptional expression of *keap1a*. Keap1 is a suppressor protein of Nrf2, which regulates the expression of oxidative response genes. A downstream target of Keap1-Nrf2, *hmox1a*, showed a markedly increased expression upon *smarca5* deletion. Moreover, overexpression of *keap1a* or knockdown of *hmox1a* partially rescued the blood clot formation, supporting that the disrupted Keap1-Nrf2 signaling in *smarca5* mutants led to the blood clot formation, thereby mimicking the venous thrombosis phenotypes. Collectively, our *smarca5*-deficient zebrafish model may serve as a new venous thrombosis model for drug screening in clinical therapy.

Results

smarca5-deficient RBCs tend to form aggregates in the CVP.

In our previously generated *smarca5*^{zko1049a} mutants (Ding et al., 2021), we observed that the blood clots were formed in CVP at 2 dpf, which was not present in their sibling embryos (Figure 1A). Our whole mount *in situ* hybridization (WISH) data showed that *scl* was expressed in blood clots, indicating that cells in the observed blood clots were primitive RBCs in *smarca5*^{zko1049a} (Figure 1B). To directly observe the blood clot formation in the CVP, we used the transgenic line (Tg) (*gata1*:dsRed/*kdrl*:GFP) to label RBCs and endothelial cells, in *smarca5*^{zko1049a} and in siblings. Confocal imaging analysis showed that the blood clots were formed inside the blood vessels (Figure 1C). Notably, there was no difference in the distribution of myeloid cells labelled by Tg (*coro1a*:GFP) or Tg (*mpo*:GFP) in caudal hematopoietic tissue (CHT) between *smarca5*^{zko1049a} and their siblings, and we did not observe accumulation of myeloid cells in the blood clots of *smarca5*^{zko1049a} (supplemental Figure 1A).

To further determine whether *smarca5* is involved in the development of primitive hematopoiesis, we examined the expression level of *gata1* and *pu.1*, which are the erythrocyte and myeloid marker genes, respectively, in *smarca5*^{zko1049a} and their siblings. WISH and quantitative PCR (qPCR) analyses showed that the expression level of *gata1* and *pu.1* was comparable between *smarca5*^{zko1049a} and their siblings at 33 hours post fertilization (hpf) (Figure 1D-E and supplemental Figure 1B-C). Moreover, the expression level of *ikaros* and *scl*, which are two primitive erythrocyte markers, was normal (Figure 1D-E), as well as the expression of globin genes in *smarca5*^{zko1049a} (Figure 1E). In addition, the myeloid markers *pu.1*, *lyz* and *mfap4* were normally expressed in *smarca5*^{zko1049a} at 33 hpf and 2 days post fertilization (dpf) (supplemental Figure 1B-C). Thus, the early development of primitive erythrocytes and myeloid cells, is not affected upon the loss of *smarca5* in zebrafish embryos.

Taken together, these results show that *smarca5* is functionally required for normal behaviors of primitive erythrocytes and the blood clotting is formed by erythrocytes in *smarca5*^{zko1049a}.

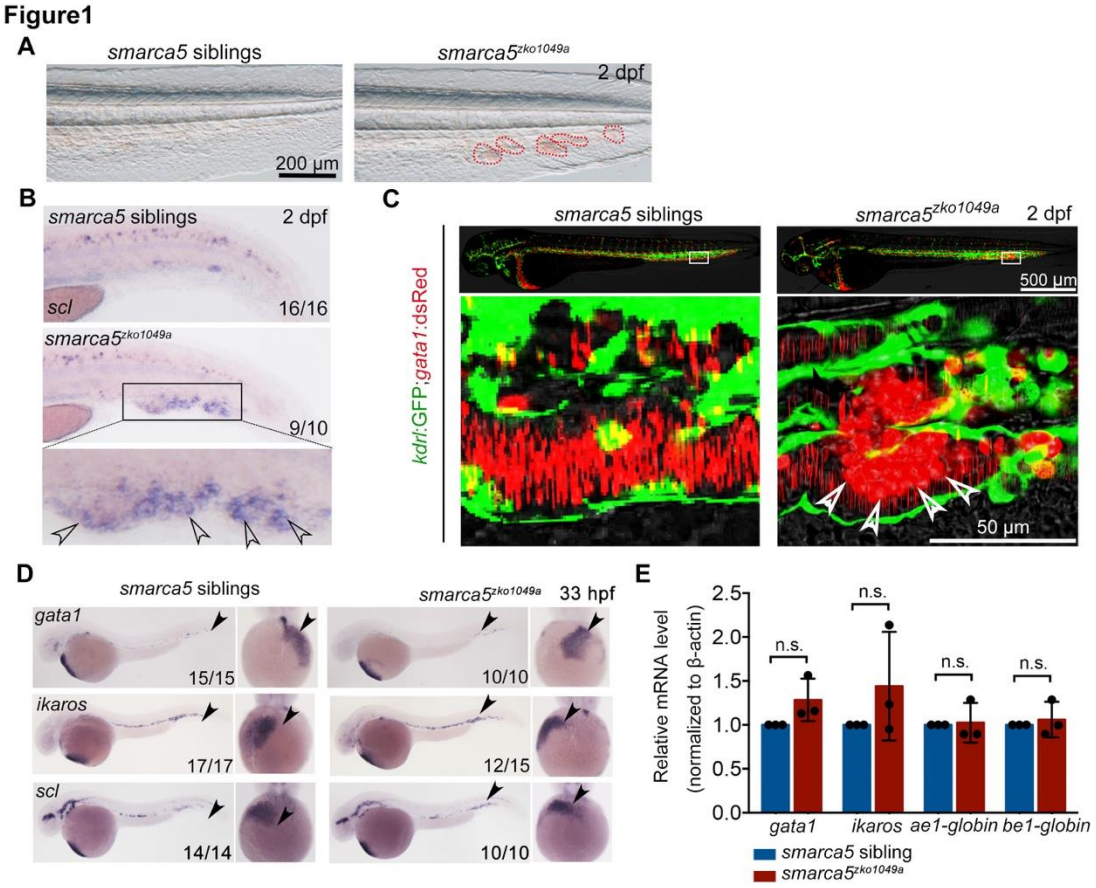

Figure 1. Blood clots occur in *smarca5*^{zko1049a}. (A) The bright-field of tail region in *smarca5*^{zko1049a} and their siblings at 2 days post fertilization (dpf). The areas circled by red dotted line show the blood clots in the caudal vein plexus. Scale bars, 200 μm. (B) Expression of *scl* at 2 dpf in *smarca5*^{zko1049a} and their siblings by WISH. The amplification region in the black rectangular box in CHT shows the enriched expression of *scl* in blood clots (indicated by arrow heads) in the caudal vein plexus. (C) The confocal imaging of transgenic line (Tg) (*kdrl*:GFP; *gata1*:dsRed) in *smarca5*^{zko1049a} and their siblings at 2 dpf. The amplification region in the white rectangular box in CHT shows the coagulation of red blood cells (RBCs) (indicated by arrow heads) in the caudal vein plexus. (D) Expression of *gata1*, *ikaros* and *scl* at 33 hours post fertilization (hpf) in *smarca5*^{zko1049a} and their siblings by WISH. (E) qPCR analysis showing the expression of *gata1*, *ikaros*, *ae1-globin* and *be1-globin* in *smarca5*^{zko1049a} and their siblings at 33 hpf. The expression level of these genes in *smarca5* siblings was set at 1. Data are mean ± s.d. (E). Asterisk presents statistical significance (n.s. not significant). *P* values were calculated by two-tailed unpaired Student's *t*-test.

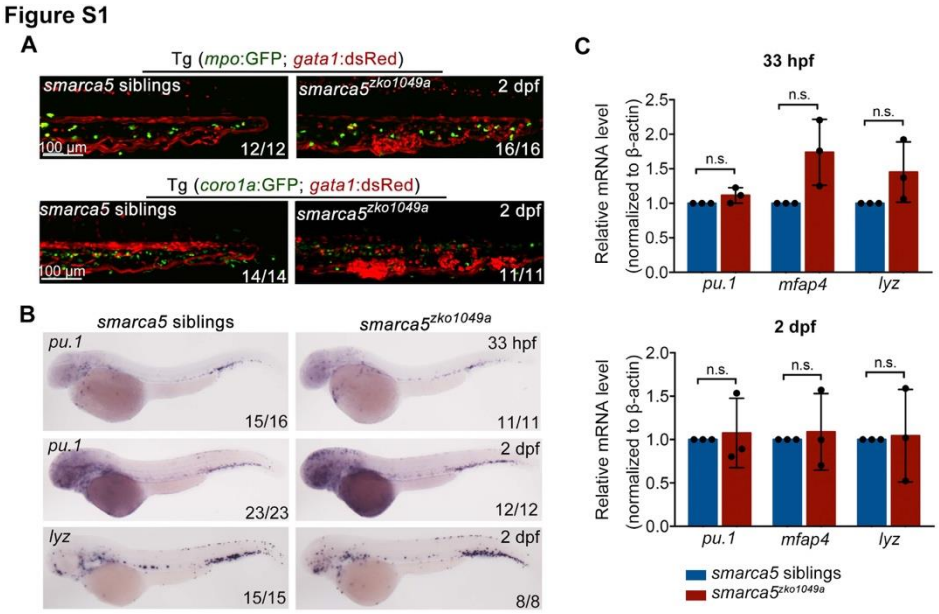

supplemental Figure 1. *smarca5* is dispensable for the development of primitive myeloid cells. (A) The confocal imaging of Tg (*mpo*:GFP; *gata1*:dsRed) and Tg (*coro1a*:GFP; *gata1*:dsRed) in *smarca5*^{zko1049a} and their siblings at 2 dpf. (B) Expression of *pu.1* and *lyz* at 33 hpf and/or 2 dpf in *smarca5*^{zko1049a} and their siblings by WISH. (C) qPCR analysis showing the expression of *pu.1*, *mfap4* and *lyz* in *smarca5*^{zko1049a} and their siblings at 33 hpf and 2 dpf. The expression level of these genes in *smarca5* siblings was set at 1. Data are mean ± s.d. (C). Asterisk presents statistical significance (n.s. not significant). *P* values were calculated by two-tailed unpaired Student's *t*-test.

The blood clots are formed by RBC aggregation that mimics venous thrombosis.

To visualize how *smarca5*-deficient RBCs formed blood clots in the CVP of *smarca5*^{zko1049a}, we performed time lapse imaging using Tg (*gata1*:dsRed). We tracked the behavior of circulating RBCs in siblings (supplemental Movie 1) and *smarca5*^{zko1049a} (supplemental Movie 2) from 36 hpf to 2 dpf. The results showed that *smarca5*-deficient RBCs tended to clump in the CVP at around 40 hpf, after which these clots will migrate or break off under blood flow at the early stage. As the blood clots formed with larger size, these clots will finally lodge in the vein (Figure 2A and supplemental Movie 2). These results show that the clumping of RBCs precedes their sequestration in CVP, suggesting that the formation of blood clots might be independent of vascular niche.

To further explore whether the blood clots formed in *smarca5*^{zko1049a} were not resulted from the abnormal niche environment, we performed parabiosis experiment using *smarca5*^{zko1049a} and their siblings and found that the blood clots were observed in both *smarca5*^{zko1049a} and their siblings in parabiosis pairs (Figure 2B). To label the RBCs in *smarca5*^{zko1049a} and their siblings, the Tg (*gata1*:dsRed) or Tg (*gata1*:GFP) transgenic line was used, respectively. The results showed that *smarca5*-deficient RBCs labelled by *gata1*:GFP aggregated both in *smarca5*^{zko1049a} and in their siblings in parabiosis pairs (Figure 2C). Although several sibling RBCs labelled by *gata1*:dsRed were found trapped in blood clots, the vast majority of *gata1*:dsRed^{+} cells were normally circulating in blood stream both in *smarca5*^{zko1049a} and their siblings (Figure 2C). Overall, these results indicate that the blood clots in *smarca5*^{zko1049a} are formed largely in RBC-autonomous manner. To further explore whether thrombocytes participate in the formation of blood clots, we detected the blood clots using Tg (*CD41*:GFP). The imaging data showed that no *CD41*:GFP^{high}-labelled thrombocytes were present in the blood clots (Figure 2D).

The CHT is a hematopoietic tissue critical for HSPC development. We thus wanted to know whether the blood clots formed in *smarca5*^{zko1049a} could influence the structure of CHT, further leading to HSPC defects. As observed previously, the structure of CHT was normal in *smarca5*^{zko1049a} and the number of *cmyb*:GFP^{+} HSPCs in CHT at 2 dpf was comparable between *smarca5*^{zko1049a} and their siblings (supplemental Figure 2A-B), indicating that the formation of blood clots in *smarca5*^{zko1049a} is dispensable for HSPC development in CHT.

Zebrafish is a useful model to screen drugs for preclinical applications. In our *smarca5*-deficient

zebrafish model, we observed blood clots in veins, raising questions regarding whether there was a thrombus-like phenotype. To this end, we tried to test the clinically used anti-thrombosis drugs to treat *smarca5*^{zko1049a} embryos. We tested reagents including heparin, aspirin and argatroban that have been reported to target thrombosis to examine whether the blood clots in *smarca5*^{zko1049a} can be alleviated after chemical treatment. The embryos were incubated in aspirin or injected with heparin or argatroban at 36 hpf and the phenotype was examined at 2 dpf. As a result, we found that a direct thrombin inhibitor, argatroban, but not an antithrombin-dependent drug, heparin, or a platelet aggregation inhibitor, aspirin, partially prevented blood clot formation in *smarca5*^{zko1049a} at 2 dpf (Figure 2E-G). These results suggest that the RBC clots in *smarca5*^{zko1049a} are more relevant to venous thrombosis and the *smarca5*-deficient zebrafish model may serve as a venous thrombosis model to screen drugs in preclinical setting.

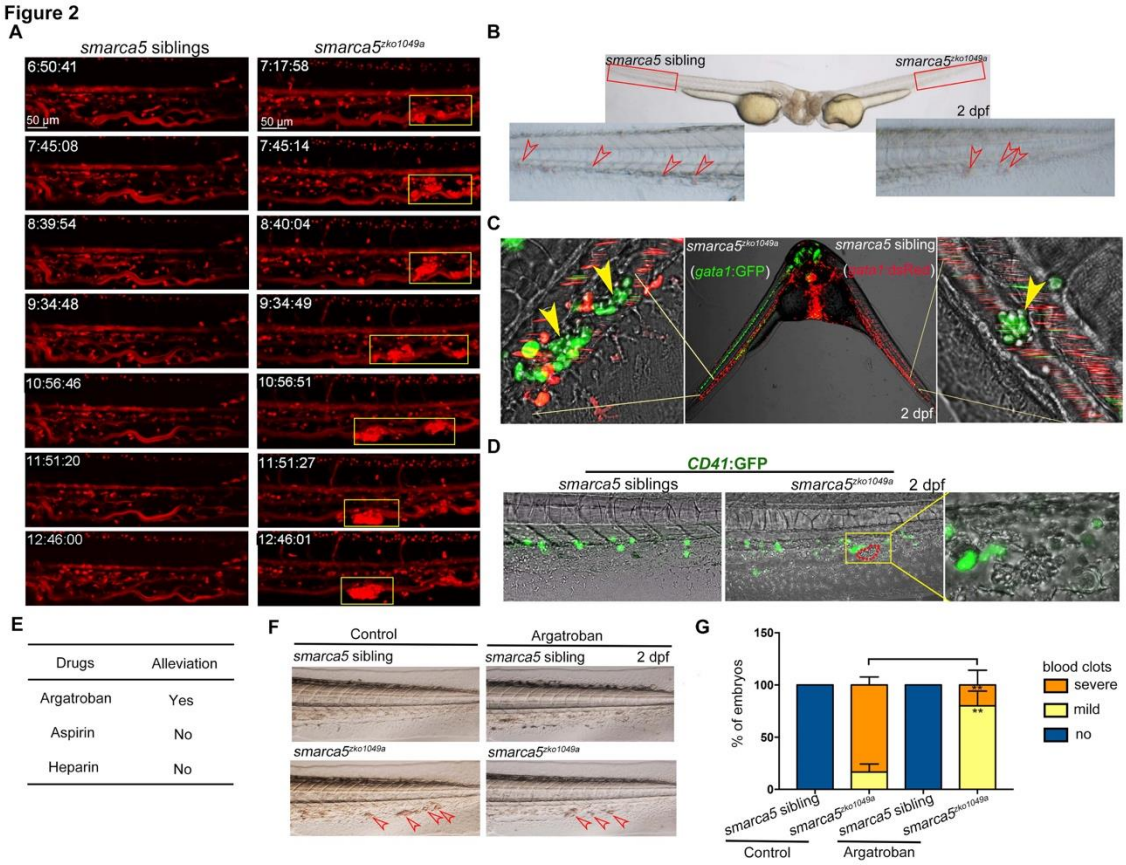

Figure 2. The Blood clots formed by RBC aggregation mimics venous thrombosis. (A) The snapshot of Tg (*gata1*:dsRed) in *smarca5*^{zko1049a} and their siblings from 36 hpf to 2 dpf. The yellow rectangular boxes in CHT show the formed blood clots *smarca5*^{zko1049a}. (B) The bright-field of parabiosis at 2 dpf between *smarca5*^{zko1049a} and their siblings. The amplification region in the red rectangular box in CHT shows the blood clots (indicated by arrow heads) in *smarca5*^{zko1049a} and their siblings. (C) The confocal imaging of parabiosis generated between *smarca5*^{zko1049a} and their siblings with Tg (*gata1*:GFP) and Tg (*gata1*:dsRed) background, respectively. The magnification in CHT shows the aggregation of *gata1*:GFP^{+} cells (indicated by arrow heads) in the caudal vein plexus. (D) The confocal imaging of Tg (*CD41*:GFP) in *smarca5*^{zko1049a} and their siblings at 2 dpf. The magnification in the yellow rectangular box in CHT shows the blood clots and the distribution of *CD41*:GFP^{+} cells. (E) Drugs used to examine whether the blood clots in *smarca5*^{zko1049a} can be alleviated. (F) The bright-field of tail region in *smarca5*^{zko1049a} at 2 dpf in control group and with argatroban treatment. The blood clots are indicated by arrow heads. (G) The quantification of blood clots phenotype in (F). Data are mean ± s.d. (G). Asterisk presents statistical significance (**p< 0.01). P values were calculated by two-tailed unpaired Student's t-test.

209

Figure S2

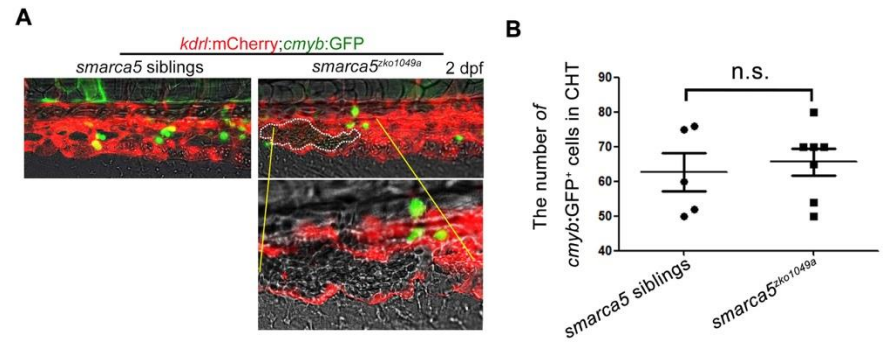

supplemental Figure 2. The RBC aggregation has no overt influence on the number of HSPCs in the CHT. (A) The confocal imaging of Tg (*kdrl*:mCherry; *cmyb*:GFP) in *smarca5*^{zko1049a} and their siblings at 2 dpf. (B) The statistical data shows the number of *cmyb*:GFP^{+} cells in the CHT in (A). Data are mean ± s.d. (B). Asterisk presents statistical significance (n.s. not significant). *P* values were calculated by two-tailed unpaired Student's *t*-test.

smarca5-deficient RBCs manifest disintegration of cristae in mitochondria.

Both quantitative and qualitative changes in RBCs have been linked to thrombosis (Weisel & Litvinov, 2019). To identify whether *smarca5* deletion will lead to the quantitative changes of RBCs, we performed fluorescence activating cell sorter (FACS) analysis of the percentage of *gata1*:dsRed^{+} cells in *smarca5*^{zko1049a} and their siblings. Deletion of *smarca5* did not lead to the significant changes in RBC counts at 2 dpf (supplemental Figure 3A-B). These data suggest that the blood clots in *smarca5*^{zko1049a} are formed by RBC aggregation with no overt cell number change.

To explore whether there exist qualitative changes in *smarca5*-deficient RBCs, we performed blood-smear and Giemsa-staining analysis. The results showed that the morphology of RBCs had no obvious changes in *smarca5*^{zko1049a} (supplemental Figure 3C). And the statistical analysis showed that the nucleocytoplasmic ratio was normal in *smarca5*-deficient RBCs (supplemental Figure 3D), indicating that the differentiation of RBCs at 2 dpf was not evidently impaired upon *smarca5* loss.

To further investigate the changes in subcellular structure of erythrocytes in *smarca5*^{zko1049a}, we performed TEM analysis. Compared with *smarca5* sibling embryos in which the circulating RBCs had normal organization in mitochondria (Figure 3A-B), we found that the *smarca5*-deficient erythrocytes displayed disintegration of cristae in mitochondria while nuclear integrity was preserved in *smarca5*^{zko1049a} (Figure 3C-E). We propose that the erythrocytes in *smarca5*^{zko1049a} may have undergone cellular damages, such as oxidative stress, which could lead to the disintegration of mitochondria (Lewerenz, Ates, Methner, Conrad, & Maher, 2018). Thus, the morphological disruption in mitochondria suggests the disorder of cellular homeostasis in erythrocytes after *smarca5* deletion.

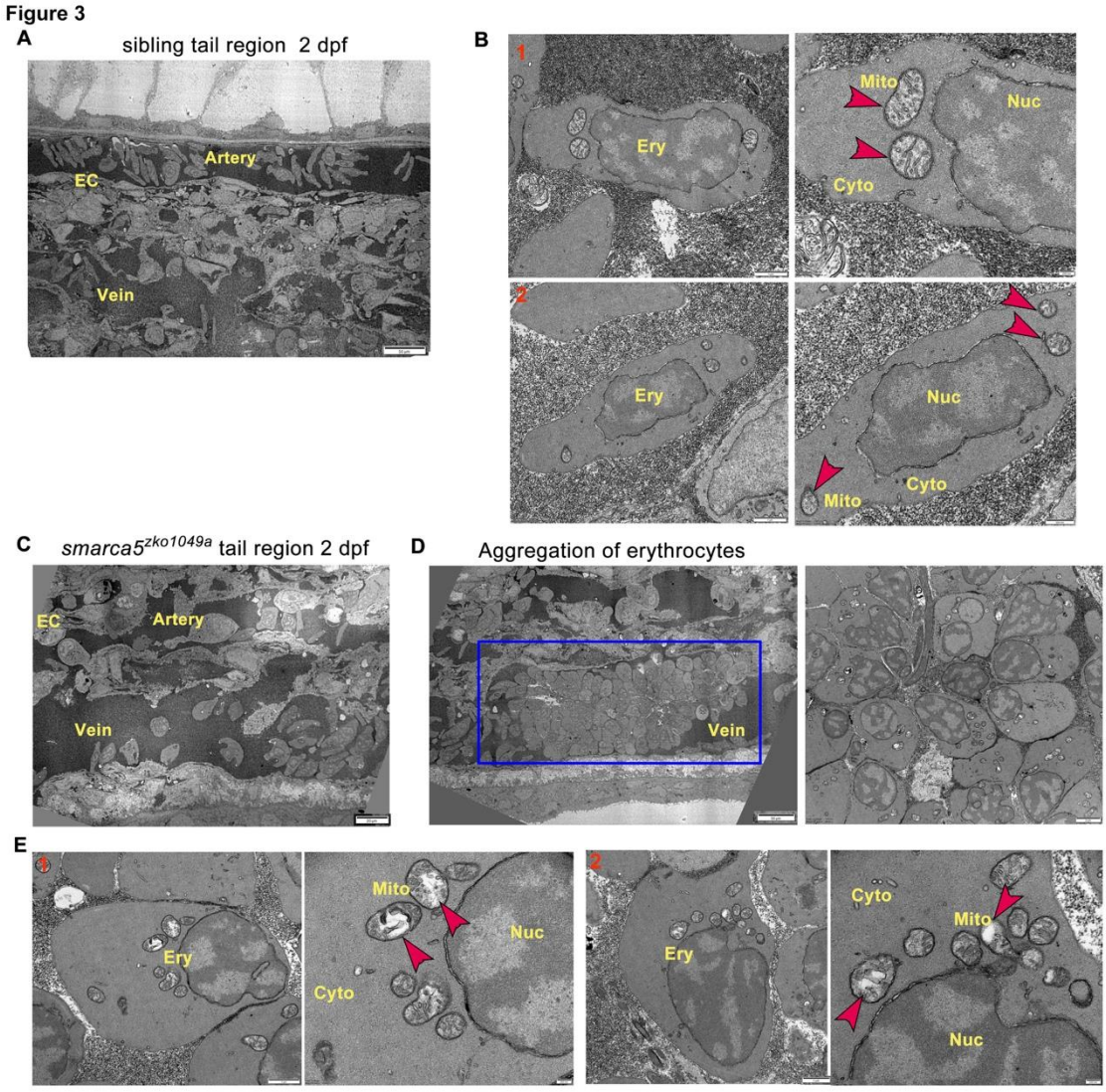

Figure 3. TEM shows abnormal organelle morphology in *smarca5*-deficient RBCs. (A) The transmission electron microscopy (TEM) view of a longitudinal section through the artery and vein plexus in sibling tail region at 2 dpf. (B) TEM view of erythrocytes in sibling embryos. The red arrow heads indicate the characteristic pattern of organization in mitochondria. (C) TEM view of a longitudinal section through the artery and vein plexus in *smarca5*^{zko1049a} tail region at 2 dpf. (D) The blue rectangular box showing blood clots in the caudal vein plexus in *smarca5*^{zko1049a}. The magnification of blood clots is shown (right). (E) TEM view of erythrocytes in *smarca5*^{zko1049a}. The red arrow heads indicate the characteristic pattern of organization in mitochondria. The disintegration of cristae in mitochondria is observed in *smarca5*-deficient RBCs. Ery, erythrocyte; EC, endothelial cell; Mito, mitochondria; Nuc, nucleus; Cyto, cytoplasm.

Figure S3

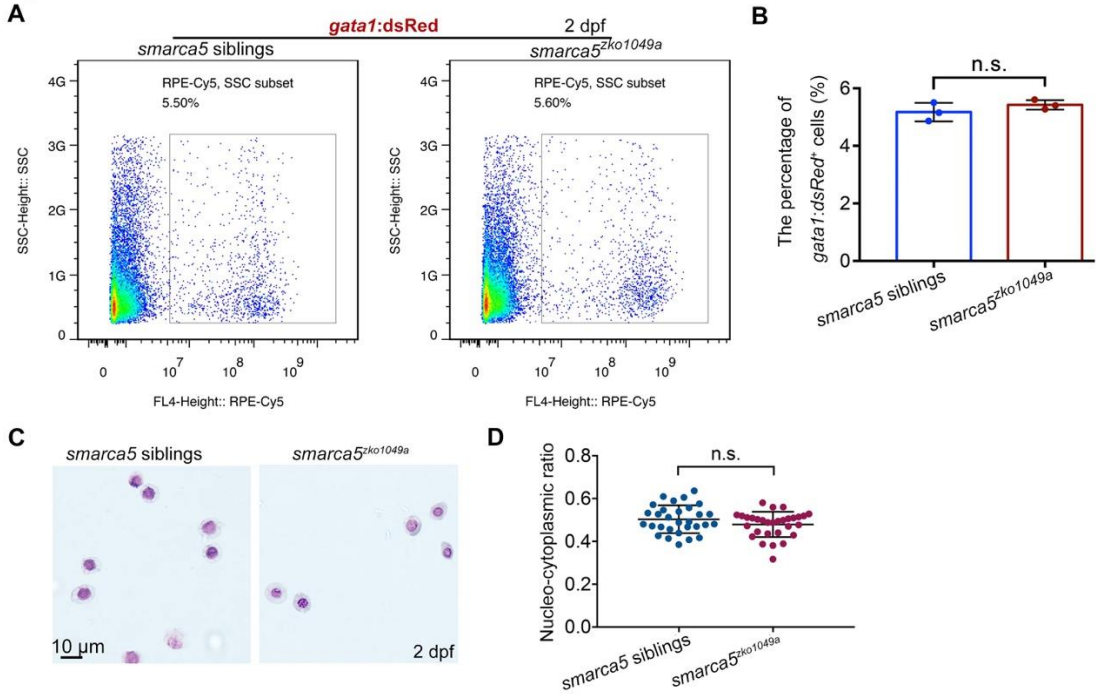

supplemental Figure 3. The morphology and number of RBCs has no obvious change in *smarca5*^{zko1049a}. (A) FACS of *gata1*:dsRed^{+} cells in wild type embryos and Tg (*gata1*: dsRed) in *smarca5*^{zko1049a} and their siblings at 2 dpf. (B) The statistical data show the percentage of *gata1*: dsRed^{+} cells in *smarca5*^{zko1049a} and their siblings in (A). (C) Blood-smear and Giemsa-staining analysis in *smarca5*^{zko1049a} and their siblings at 2 dpf. Scale bar, 10 μm. (D) Scatter plots showing the nucleocytoplasmic ratio in RBCs from *smarca5*^{zko1049a} and their siblings. Data are mean ± s.d. (B and D). Asterisk presents statistical significance (n.s. not significant). *P* values were calculated by two-tailed unpaired Student's *t*-test.

Transcriptional dysregulation of genes related to erythrocyte function and homeostasis after *smarca5* deletion.

Smarca5 typically regulates nucleosome spacing, further affecting gene transcription (Clapier, Iwasa, Cairns, & Peterson, 2017). To decipher how loss of Smarca5 affects the transcriptome, RNA-seq was used to profile sorted erythrocytes labelled by *gata1*:dsRed from *smarca5*^{zko1049a} and their siblings at 2 dpf, respectively (Figure 4A). Principal components analysis (PCA) indicated clear separation of the *smarca5*^{zko1049a} and sibling samples (supplemental Figure 4A). 1,506 genes were upregulated and 633 genes were downregulated significantly (Log2(fold change) > 1, adjusted *P*-value < 0.05) in *smarca5*-deficient erythrocytes compared to erythrocytes from siblings (Figure 4B).

Gene set variation analysis (GSVA) revealed a strong enrichment of terms related to 'Gata1 targets', 'autophagy', 'erythrocytes take up carbon dioxide and release oxygen' and 'erythrocytes take up oxygen and release carbon dioxide' in sibling erythrocytes; for *smarca5*^{zko1049a}, while the 'apoptosis', 'environmental stress response', 'senescence' and 'cell oxidation' were markedly increased (Figure 4C). The enrichment plots showed the decreased expression of genes related to 'erythrocyte homeostasis' in *smarca5*^{zko1049a}, whereas the expression of genes related to 'inflammatory response' was increased (Figure 4D). These results suggest that the disrupted pathways in *smarca5*-deficient RBCs were highly related to erythrocyte function and cellular homeostasis.

RBCs have specialized proteome, which is enriched in hemoglobin. We then focused on the expression of hemoglobin complex related genes. The expression of genes related to the hemoglobin complex, including *hbbe1.1*, *hbbe1.3*, *hbbe2*, and *hbae3*, was slightly decreased in *smarca5*^{zko1049a} (supplemental Figure 4B). However, the level of hemoglobin detected by O-dianisidine staining was comparable between *smarca5*^{zko1049a} and their siblings (supplemental Figure 4C). Therefore, the slightly decreased expression of hemoglobin complex related genes after *smarca5* deletion does not lead to obvious hemoglobinopathy in *smarca5*^{zko1049a} at 2 dpf.

In addition, we observed the persistent expression of *spi1a*, *spi1b*, *mfap4* and *lyz* markers characteristic of myeloid cells in *smarca5*-defecient erythrocytes (supplemental Figure 4D). Perturbation of the exquisite control by *smarca5* likely causes "hybrid" primitive erythrocytes that resemble partial transcriptional properties of myeloid cells. One possible mechanism for this

293 phenotype is the regulation of SMARCA5 and CTCF at the enhancer of PU.1 (Dluhosova et al.,
294 2014), thereby blocking of *smarca5* leads to the upregulation of *pu.1* gene expression. However,
295 despite the inappropriate expression of myeloid genes in *smarca5*-deficient RBCs, the
296 development of myeloid lineage was not obviously impaired in *smarca5*^{zko1049a} manifested with
297 normal expression pattern of *pu.1* and *lyz* at 33 hpf and 2 dpf (supplemental Figure 1A-B),
298 suggesting the unaltered lineage choices at the primitive stage. To further explore whether the
299 inappropriate expression of myeloid genes in *smarca5*-deficient RBCs caused RBC aggregation,
300 we tried knockdown of *pu.1* in *smarca5*^{zko1049a}. The results showed that knockdown of *pu.1*
301 cannot rescue the RBC aggregation phenotype in *smarca5*^{zko1049a} (supplemental Figure 4E-F).
302 Taken together, *smarca5* deletion leads to the disrupted pathways related to erythrocyte function
303 and cellular homeostasis.
304

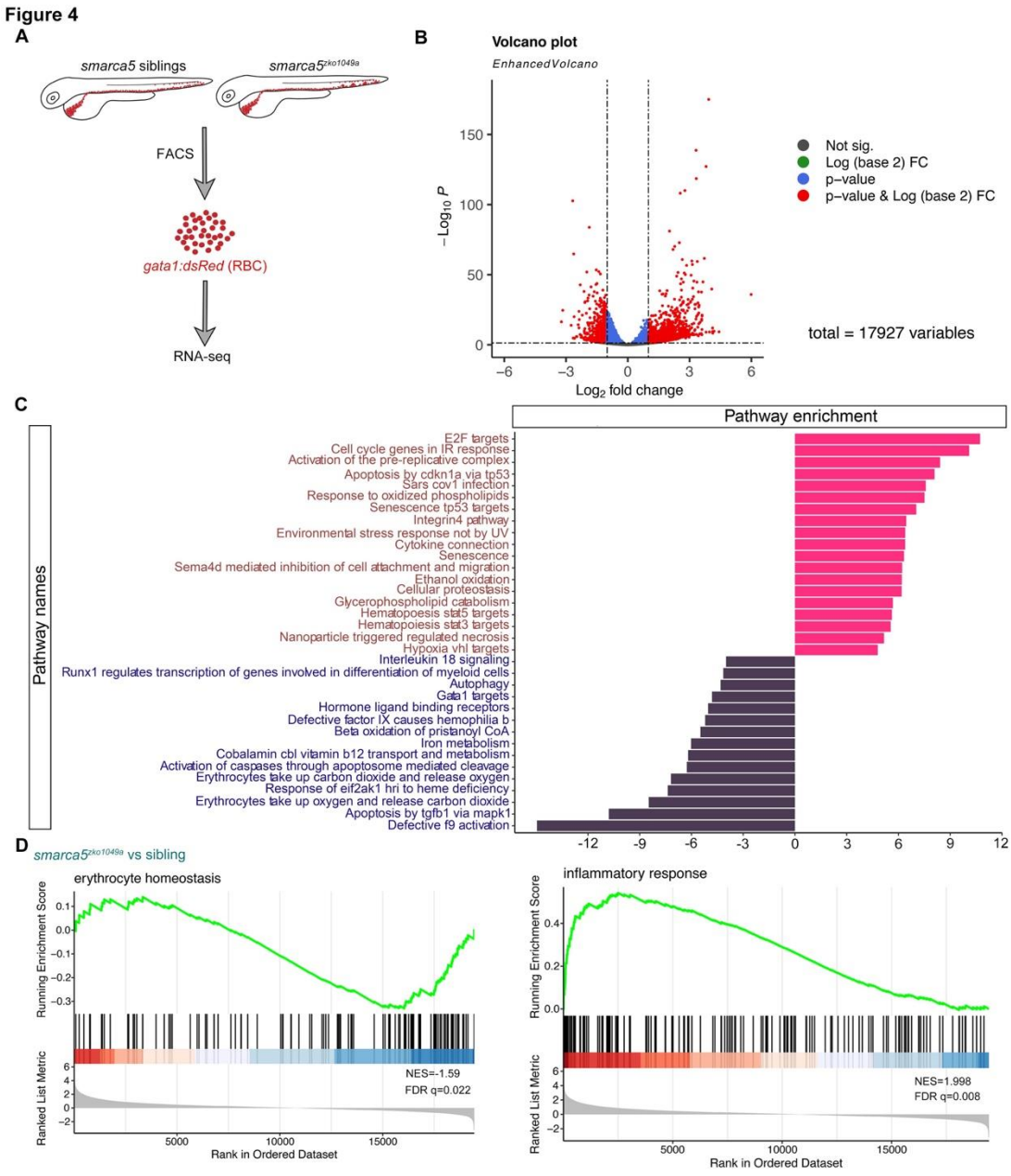

Figure 4. Transcriptional disruption of genes related to erythrocyte function and homeostasis after *smarca5* deletion. (A) Schematic representation of the RBC RNA-seq workflow in *smarca5*^{zko1049a} and their siblings at 2 dpf. (B) Volcano plot showing differential expression genes between RBCs from *smarca5*^{zko1049a} and their siblings by Deseq2. −Log10 P, negative log10 adjusted P-value. Adjusted P-value < 0.05, log2 fold change>1. (C) Differential pathway enriched in RBCs from *smarca5*^{zko1049a} and their siblings by GSVA. The x axis represents the t values of GSVA scores. Two-sided unpaired limma-moderated t test. (D) Enrichment plots for the top pathways in the mutant RBCs by GSEA.

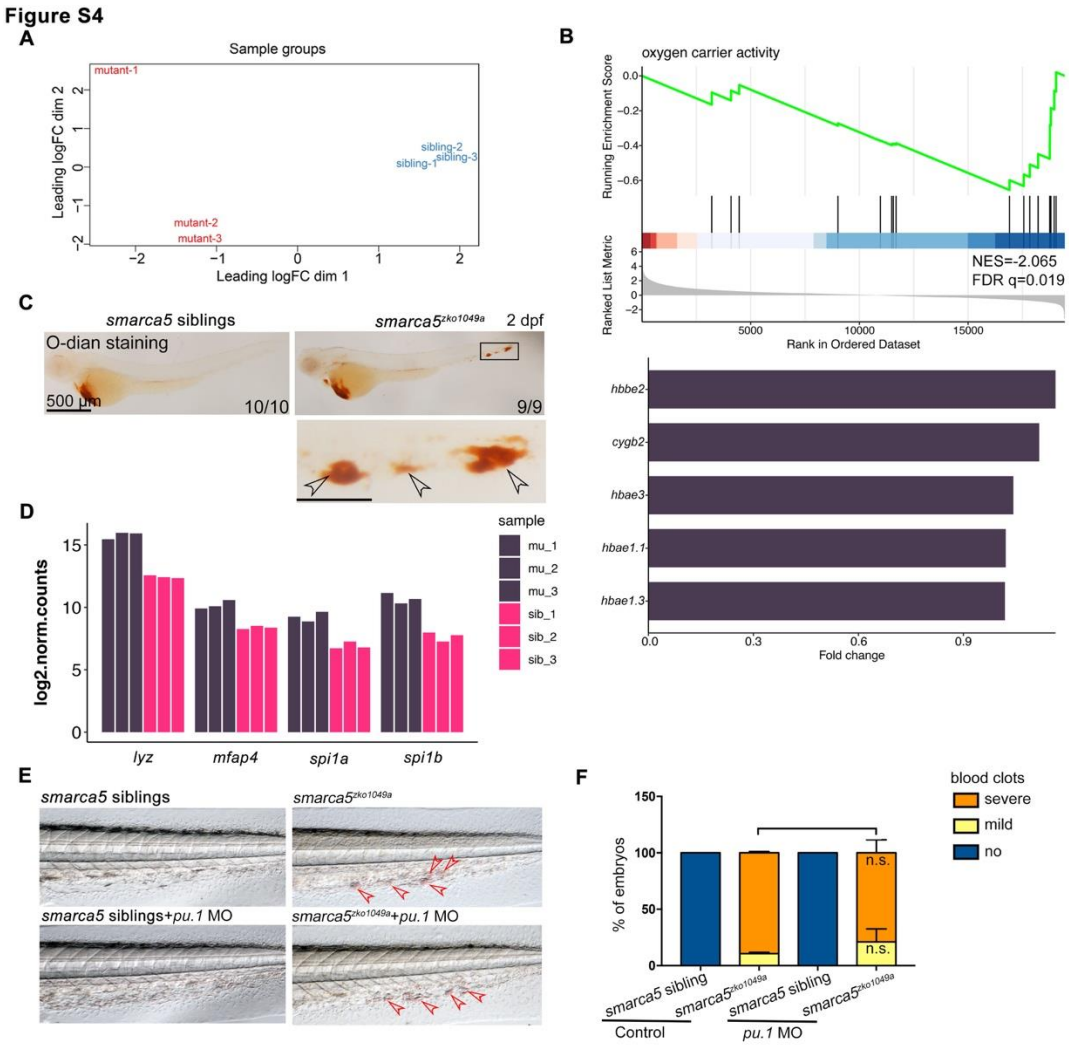

315

316 **supplemental Figure 4. RNA-seq analysis for RBCs in *smarca5*^{zko1049a} and their siblings.** (A)
317 Principal components analysis (PCA) plot of biological replicates by the transcriptional data. (B)
318 Enrichment plot for the pathway in sibling RBCs by GSEA (top) and bar plot showing the
319 pathway specific highly expressed genes (bottom). Fold change, $\log_2$ fold change. The genes are
320 sorted by the values of $\log_2$ fold change. (C) *O*-dianisidine staining in *smarca5*^{zko1049a} and their
321 siblings at 2 dpf. The amplification region in the black rectangular box in CHT shows the blood
322 clots (indicated by arrow heads) in *smarca5*^{zko1049a}. (D) Bar plot showing the gene counts of *lyz*,
323 *mfap4*, *spi1a* and *spi1b* in RBCs from *smarca5*^{zko1049a} and siblings. (E) The bright-field of tail
324 region in *smarca5*^{zko1049a} at 2 dpf in control group and with *pu.1* MO injection. The blood clots are
325 indicated by arrow heads. (F) The quantification of blood clots in (E). Data are mean ± s.d. (F).
326 Asterisk presents statistical significance (n.s. not significant). *P* values were calculated by
327 two-tailed unpaired Student's *t*-test.

328

Deletion of *smarca5* disrupts chromatin accessibility in RBCs.

To explore the mechanism through which Smarca5 in regulating the chromatin accessibility in RBCs, we performed the ATAC-seq in FACS-purified RBCs from *smarca5*^{zko1049a} and their siblings at 2 dpf. Density heatmaps of mapped ATAC-seq reads showed that fragments less than 100 bp in length clustered immediately upstream of transcriptional start sites (TSSs) throughout the zebrafish genome in both mutant and sibling RBC nuclei (supplemental Figure 5A-B). The PCA analysis was performed for ATAC-seq samples and the results showed that the mutant samples or sibling samples can be grouped together, respectively (supplemental Figure 5C). The feature distributions of mutant-ATAC-seq peaks and sibling-ATAC-seq peaks across the genome were identified by ChIPseeker (supplemental Figure 5D).

We then calculated the number of genes with changes in chromatin accessibility after *smarca5* deletion (Figure 5A). The chromatin accessibility at promoters of 256 genes was decreased in *smarca5*^{zko1049a}, while there were 439 genes with increased chromatin accessibility at promoters after *smarca5* deletion. Next, we screened the motifs enriched in sibling RBC-specific accessible chromatin regions. We found that the erythrocyte master regulator-Gata1 motif was on the top list (Figure 5B). Thus, deletion of *smarca5* might affect the binding of hematopoietic transcription factors in erythrocytes, such as Gata1. It has been reported that Smarca5 could interact with Gata1 in erythrocytes (Rodriguez et al., 2005). We propose that Smarca5 might be recruited by Gata1 and mediate the chromatin accessibility of Gata1 binding sites in target genes.

We further detected the genes in which the chromatin accessibility at promoters and their transcription were both increased or decreased after *smarca5* deletion (Figure 5C). The results showed that the chromatin accessibility and transcription of 84 genes, such as *il34*, *cox4i2*, *skap2*, *vclb*, and *acbd7*, were increased, while the chromatin accessibility and transcription of 36 genes, such as *trim2a*, *keap1a*, *skap2*, *acox3*, *igfbp1a* and *ada*, were decreased in *smarca5*-deficient RBCs (Figure 5D). Taken together, *smarca5* deletion leads to the disrupted chromatin accessibility and transcriptome in RBCs.

Figure 5

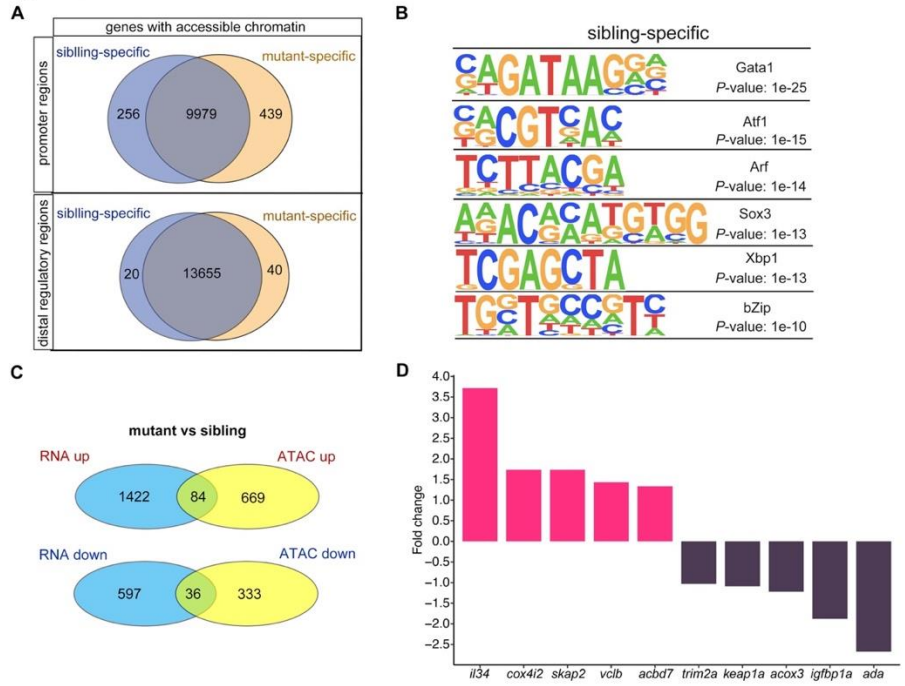

Figure 5. Changes in chromatin accessibility in RBCs from *smarca5*^{zko1049a} and their siblings. (A) Venn plot showing the genes of sibling and mutant specific accessible chromatin regions at promoter and distal regulator regions, respectively. (B) Motifs enriched in nucleosome free regions (NFRs) with lost accessibility after smarca5 deletion. (C) Venn plot showing the overlap of genes with specific accessible chromatin regions and up-regulated expression in mutant (top) and sibling (bottom) RBCs, respectively. Genes for ATAC-seq were assigned by differential accessible regions. (D) Bar plot showing the selected sibling and mutant specific differential expression genes. Fold change, $\log_2$ fold change.

Figure S5

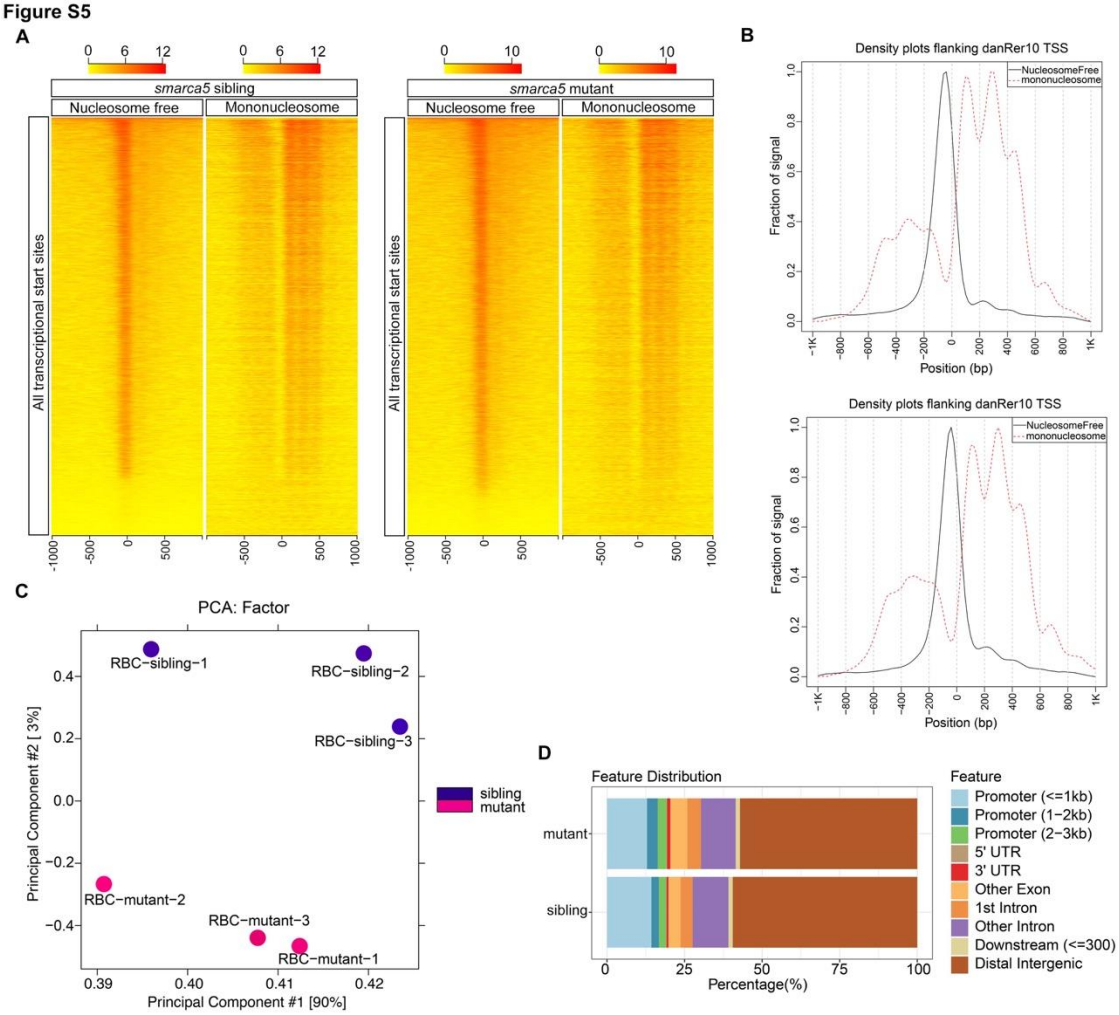

supplemental Figure 5. ATAC-seq analysis for RBCs in *smarca5*^{zko1049a} and their siblings. (A) Heatmaps showing density of mapped ATAC-seq reads from single biological replicates 1 kb up and downstream of transcriptional start sites (TSS) in danRer10. Separate heatmaps for fragments of nucleosome free (less than 100 bp) and mononucleosome (between 180 and 247 bp) are shown. (B) Density plots flanking danRer10 TSS from sibling and mutant RBCs for mapped reads shown in (A). (C) PCA plot of biological replicates using all ATAC-seq peaks. (D) Bar plot drew by ChIPseeker showing the feature distributions of mutant-ATAC-seq peaks and sibling-ATAC-seq peaks across the genome.

keap1a acts as a downstream target of Smarca5 in RBC aggregation.

Based on the screening results, the chromatin accessibility at *keap1a* promoters, which contains Gata1 motif, was decreased in *smarca5*^{zko1049a} (Figure 6A). The transcription level of *keap1a* detected by qPCR was also decreased in *smarca5*-deficient RBCs (Figure 6B). Given that *keap1* was previously identified to correlate with human venous thrombosis (Akin-Bali, Eroglu, Ilk, Egin, & Kankilic, 2020), we propose that *keap1a* may act as a downstream target of Smarca5 in RBCs. Keap1-Nrf2 system is an evolutionarily conserved defense mechanism in oxidative stress (Itoh et al., 1997; Itoh et al., 1999). In cytoplasm, Keap1 could anchor to Nrf2 to facilitate the Nrf2 degradation, while oxidative stress leads to the proteasomal degradation of Keap1 and release of Nrf2 to the nucleus, thereafter activate the expression of oxidation defense factors. Both our RNA-seq and qPCR analysis showed the downregulation of *keap1a* and as a downstream target of Nrf2, *hmox1a* showed a markedly increase in gene expression upon *smarca5* deletion (Figure 6C), suggesting the disruption of Keap1-Nrf2 signaling pathway. It is worthy of note that, although the upregulated expression of Keap1-Nrf2 downstream targets can protect cells from oxidative damage, the excessive activation of *hmox1a*, which catalyzes the degradation of heme to biliverdin, carbon monoxide, and $Fe2^{+}$, could even lead to the oxidative stress (Hassannia, Vandenabeele, & Vanden Berghe, 2019). Thus, we propose that the unbalanced Keap1-Nrf2 signaling, especially the upregulation of *hmox1a*, could increase oxidative damage in *smarca5*-deficient RBCs. We next performed functional validation of *keap1a* in *smarca5*^{zko1049a} by overexpression of *hsp70*:*keap1a*-EGFP. Heat shock was performed at 24 hpf and 36 hpf, and the phenotype was examined at 2 dpf. The results showed that overexpression of *keap1a* in *smarca5*^{zko1049a} could partially rescue the blood clots phenotype (Figure 6D-E). In addition, knockdown of *hmox1a*, the downstream target of Keap1-Nrf2, can also partially rescue the blood clots phenotype in *smarca5*^{zko1049a} (Figure 6F-G), further supporting that the Keap1-Nrf2 signaling pathway downstream of Smarca5 is essential for blood clot formation.

To further identify the conserved role of *SMARCA5* in mammalian erythrocyte homeostasis, we used K562 cells (human erythroleukemic cells) to perform further analysis. Treatment of hemin induced the hemoglobinization of most K562 cells, suggesting the efficient erythroid differentiation (supplemental Figure 6A-B). We then knocked down *SMARCA5* in hemin-induced K562 cells using *SMARCA5* short interfering RNA (siRNA) and the qPCR and western blot

406 analyses showed that both the RNA and protein levels of *SMARCA5* were decreased significantly
407 after si*SMARCA5*s (si*SMARCA5*-1, si*SMARCA5*-2 and si*SMARCA5*-3) transfection (supplemental
408 Figure 6C-D). In addition, the expression of *HMOX1* was obviously upregulated after *SMARCA5*
409 knockdown (supplemental Figure 6E), indicating the conserved role of *SMARCA5* in human
410 erythrocyte homeostasis.
411 Considering the role of Keap1-Nrf2 signaling pathway in oxidative stress regulation, we further
412 asked whether the oxidative stress could be a trigger for blood clot formation in *smarca5* mutants.
413 Then, we used a free radical scavenger glutathione to determine the mechanisms of
414 *smarca5*-deficiency induced blood clots. We found that glutathione obviously prevented
415 thrombosis in *smarca5*^{zko1049a} (supplemental Figure 7A-B), implying that free radical generation
416 may play an important role in thrombosis in *smarca5*^{zko1049a}.
417 Taken together, loss of *smarca5* leads to the disruption of *keap1a* expression and excessive
418 activation of *hmox1a* in *smarca5*^{zko1049a}, which together contribute to the formation of blood clots.
419

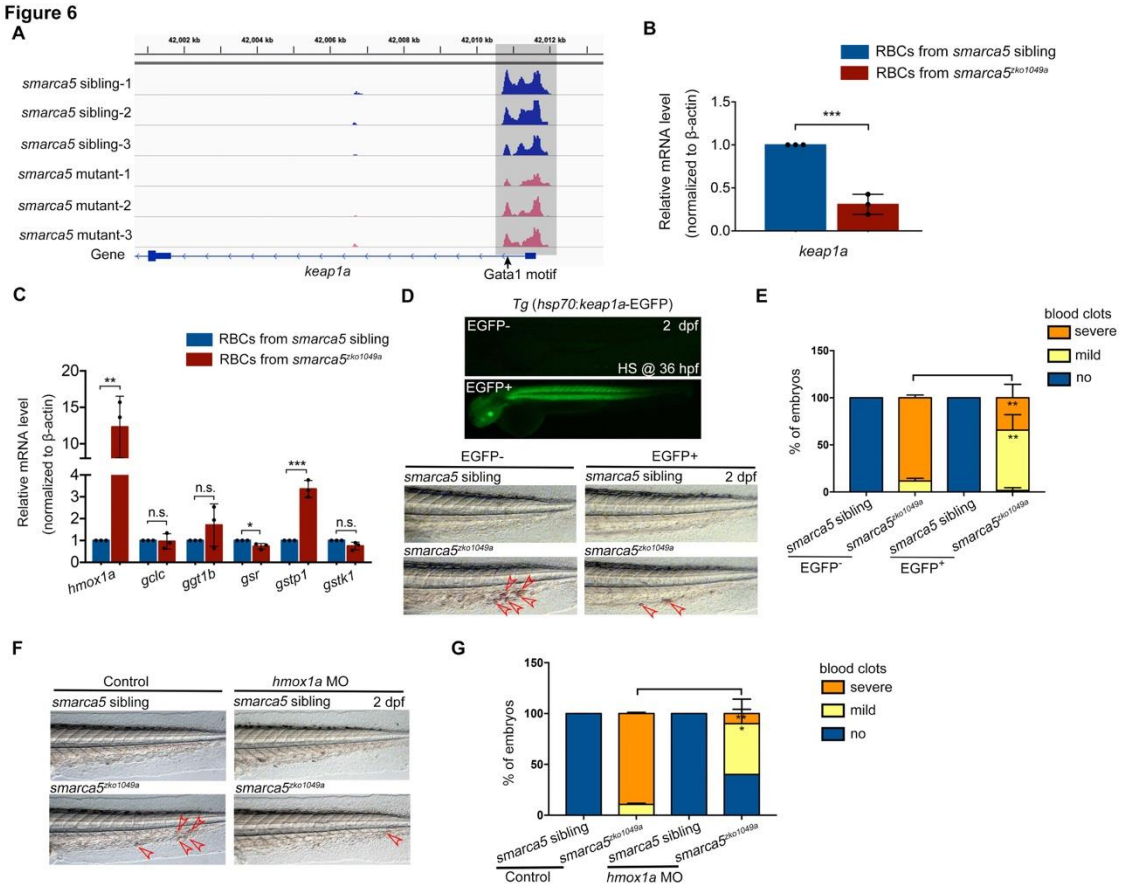

Figure 6. Keap1- Nrf2 signaling pathway acts at downstream of Smarca5 in regulating RBC aggregation. (A) The browser views showing the ATAC-seq peaks in *keap1a* promoter with in *smarca5*^{zko1049a} and their siblings. Gray box indicates the change of ATAC-seq peaks after *smarca5* deletion. The location of Gata1 motif at *keap1a* promoter is indicated by arrow. (B) qPCR analysis showing the expression of *keap1a* in RBCs from *smarca5*^{zko1049a} and their siblings at 2 dpf. (C) qPCR analysis showing the expression of *hmox1a*, *gclc*, *ggt1b*, *gsr*, *gstp1* and *gstk1* in RBCs from *smarca5*^{zko1049a} and their siblings at 2 dpf. (D) The imaging of EGFP fluorescence in Tg (*hsp70*:*keap1a*-EGFP) embryos at 2 dpf. Heat shock was performed at 36 hpf. The bright-field of tail region in *smarca5*^{zko1049a} and their siblings, with or without Smarca5 overexpression at 2 dpf. (E) The quantification of blood clots phenotype in (D). (F) The bright-field of tail region in *smarca5*^{zko1049a} and their siblings, in control group and with *hmox1a* MO injection. The blood clots are indicated by arrow heads. (G) The quantification of blood clots phenotype in (F). Data are mean ± s.d. (B, C, E, G). Asterisk presents statistical significance (*p< 0.05, **p< 0.01, ***p< 0.001, n.s. not significant). *P* values were calculated by two-tailed unpaired Student's *t*-test.

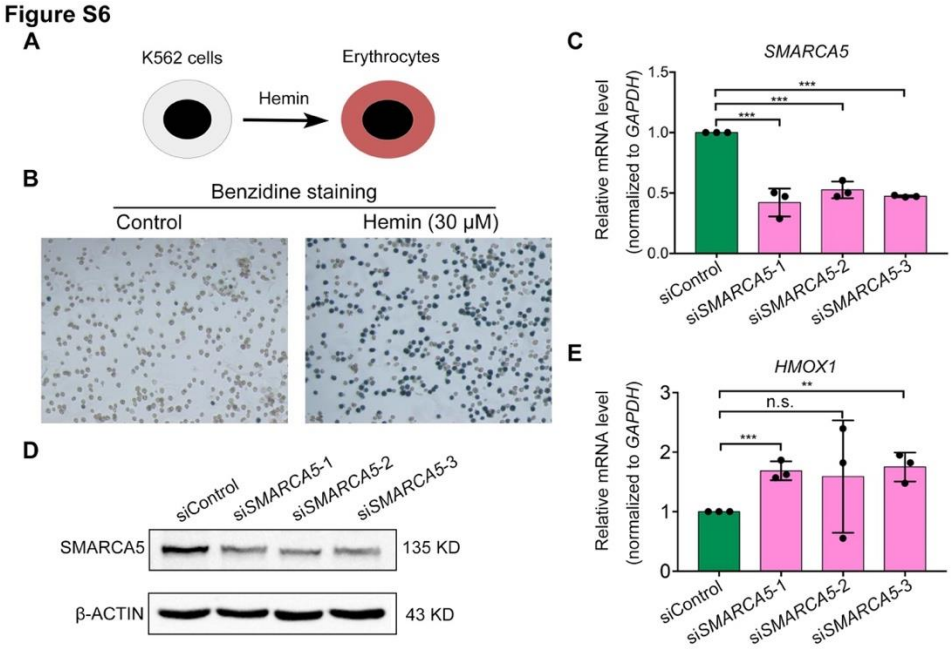

supplemental Figure 6. The upregulation of *HMOX1* in hemin-induced K562 cells after knockdown of *SMARCA5*. (A) Schematic representation the induction of erythroid differentiation of K562 cells using hemin. (B) Benzidine staining of K562 cells in control group and with hemin treatment. (C) qPCR analysis showing the expression of *SMARCA5* in control (siControl) and after *SMARCA5* knockdown (si*SMARCA5*-1, si*SMARCA5*-2, si*SMARCA5*-3). The expression level of *SMARCA5* was normalized to *GAPDH*. (D) Western blot showing the protein level of SMARCA5 in control and after *SMARCA5* knockdown. (E) qPCR analysis showing the expression of *HMOX1* in control and after *SMARCA5* knockdown. The expression level of *HMOX1* was normalized to *GAPDH*. Data are mean ± s.d. (C and E). Asterisk presents statistical significance (**p< 0.01, ***p< 0.001, n.s. not significant). *P* values were calculated by two-tailed unpaired Student's *t*-test.

Figure S7

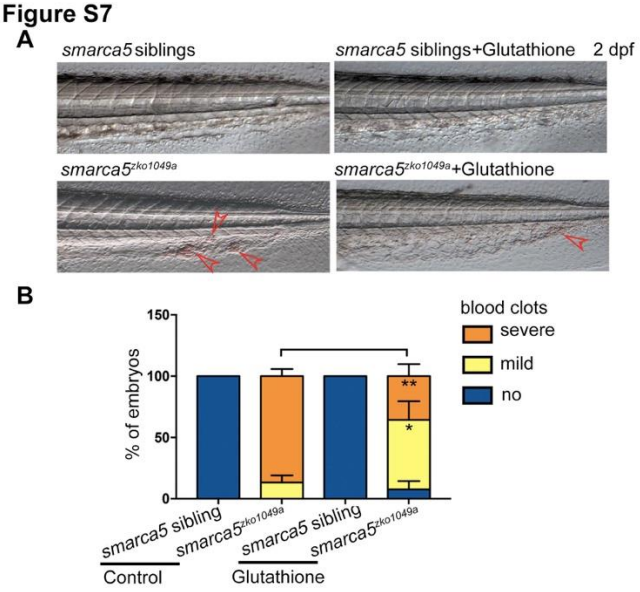

supplemental Figure 7. The free radical generation may play a major role in RBC aggregation in *smarca5*^{zko1049a}. (A) The bright-field of tail region in *smarca5*^{zko1049a} at 2 dpf in control group and with glutathione treatment. The blood clots are indicated by arrow heads. (B) The quantification of blood clots phenotype in (A). Data are mean ± s.d. (B). Asterisk presents statistical significance (*p< 0.05, **p< 0.01). *P* values were calculated by two-tailed unpaired Student's *t*-test.

Discussion

In this work, we develop a zebrafish thrombosis model with a deletion of an epigenetic regulator-*smarca5*. The blood clots are formed in the CVP of *smarca5*^{zko1049a} and the erythrocytes manifest disintegration of cristae in mitochondria. Further transcriptome and chromatin accessibility analysis show that *keap1a* acts as a downstream target of Smarca5. Moreover, the elevated expression of the downstream target of Keap1-Nrf2, *hmox1a*, leads to the aggregation of *smarca5*-deficient RBCs. Together, these results demonstrate the protective role of Smarca5 in regulating erythrocyte homeostasis and that the *smarca5* loss-of-function zebrafish mutant may serve as a new thrombosis model to screen molecular drugs for clinical therapy.

Considering the conserved coagulation and anticoagulation signaling pathway, the zebrafish model has been used to study the physiology of thrombosis (Hanumanthaiah, Day, & Jagadeeswaran, 2002; Jagadeeswaran, Sheehan, Craig, & Troyer, 1999; Sheehan et al., 2001). The ferric chloride and laser injury methods are widely used in zebrafish to generate thrombus in the circulation (M. Gregory, Hanumanthaiah, & Jagadeeswaran, 2002). Phenylhydrazine-treated zebrafish also develop thrombosis in the caudal vein (Zhu et al., 2016). Moreover, zebrafish is an ideal model to explore novel players in thrombosis based on genetic manipulation. For example, mutation of *anti-thrombin III* gene in zebrafish can mimic disseminate intravascular coagulation (Liu et al., 2014). miR-126 was identified as a regulator of thrombi generation in zebrafish (Zapilko et al., 2020). Importantly, the transparency of zebrafish embryo makes it feasible to image the kinetics of thrombus formation. In our study, the *gata1*:dsRed labelled RBCs were imaged during blood clot formation. Thus, the zebrafish thrombosis model is a great asset for exploring the underlying mechanisms in thrombosis formation.

Unlike Brg1, which is essential for mouse erythrocyte development by regulating globin gene expression (Bultman et al., 2005; Griffin et al., 2008), Smarca5 is required for primitive erythrocyte homeostasis at the erythrocyte differentiation stage. Deletion of *smarca5* does not lead to the gross changes in RBC morphology and viability, but specifically results in the RBC aggregation phenotype. The mechanistic details for different chromatin remodelers functioning in the different processes during erythropoiesis warrant further investigation.

Previous evidence suggests that chromatin remodeler NuRD is required to maintain lineage fidelity during erythroid-megakaryocyte ontogeny (Gao et al., 2010; G. D. Gregory et al., 2010).

Our results show that, despite the normal lineage choice for primitive erythrocytes in *smarca5*^{zko1049a}, the aberrant activation of myeloid genes occurred in RBCs after *smarca5* deletion. The exquisite cell lineage control by *smarca5* may be due to the regulation of SMARCA5 at the enhancer of PU.1 (Dluhosova et al., 2014).

Besides the conserved role of Keap1-Nrf2 system in oxidative stress, Keap1-Nrf2 is also demonstrated to act as a regulator in cell development and differentiation across multiple tissues and cell types. For instance, Keap1-Nrf2 signaling pathway is indispensable for hematopoietic stem cell (HSC) lineage commitment in mice (Murakami, Shimizu, Romeo, Yamamoto, & Motohashi, 2014). Knockout of *Keap1* in HSCs showed enhanced granulocyte-monocyte differentiation ability at the expense of lymphoid and erythrocyte differentiation. And the expression level of erythrocyte and lymphoid genes was decreased in *Keap1*-deficient HSCs. Importantly, the abundance of Hmox1 is upregulated during erythrocyte differentiation, and Hmox1 expression must be tightly regulated at appropriate level for efficient erythropoiesis (Garcia-Santos et al., 2014). Overexpression of Hmox1 impairs hemoglobin synthesis, while lack of Hmox1 leads to the enhancement of hemoglobinization. Here, we show that the disruption of *keap1a* expression and excessive activation of *hmox1a* in *smarca5*^{zko1049a} contribute to RBC aggregation. Besides the free radical generation, which may play an important role in RBC aggregation in *smarca5*^{zko1049a}, we cannot rule out other possibilities that maybe also involved in the observed phenotype, such as the regulation of Keap1-Nrf2 signaling pathway in erythrocyte gene expression.

In summary, we have demonstrated, for the first time, that deletion of *smarca5* in zebrafish leads to the formation of blood clots that mimics venous thrombosis by regulating the Keap1-Nrf2 signaling pathway in RBCs. These findings raise the possibility that zebrafish *smarca5* mutant may serve as a new venous thrombosis model for drug screening and pre-clinical therapeutic assessment.

Methods

Zebrafish strains

Zebrafish strains including Tubingen, Tg (*CD41*:GFP) (Lin et al., 2005), Tg (*gata1*:dsRed) (Traver et al., 2003), Tg (*kdrl*:mCherry) (Bertrand et al., 2010), Tg (*mpo*:GFP) (Renshaw et al., 2006), Tg (*coro1a*:GFP) (L. Li, Yan, Shi, Zhang, & Wen, 2012), *smarca5*^{zko1049a} heterozygous mutants (Ding et al., 2021) were raised under standard conditions (28.5°C in system water). The zebrafish embryos were raised in incubator at 28.5°C. The present study was approved by the Ethical Review Committee of the Institute of Zoology, Chinese Academy of Sciences, China.

Whole mount *in situ* hybridization (WISH)

WISH was performed as previously described (Wang et al., 2011). The Digoxigenin-labelled RNA probe genes including *gata1*, *ikaros*, *scl*, *pu.1*, and *lyz* were cloned from zebrafish cDNA and ligated to the T-vector, then *in vitro* transcribed using T7 or SP6 polymerase.

Quantitative PCR (qPCR)

Total RNAs were extracted from *smarca5*^{zko1049a} and their sibling embryos using TRIzol reagent (Life technologies, 15596018) or from sorted RBCs using QIAGEN RNeasy Mini Kit (Cat. No. 74104). The cDNA was reverse transcribed using M-MLV Reverse Transcriptase (Promega, M1701). The detailed primers used for qPCR are listed in Supplementary file 1A.

Morpholinos (MOs)

The antisense MOs were purchased from GeneTools. The sequences of MOs were used as previous described, these gene-specific MOs include *hmox1a* MO and *pu.1* MO. The detailed sequence and dosage used in this work are listed in Supplementary file 1B.

Parabiosis experiment

Parabiosis experiment was performed by following the previous published procedures (Demy et al., 2013; Hagedorn et al., 2016). Briefly, *smarca5*^{zko1049a} and their sibling embryos between the 128-cell blastula and 30% epiboly stages were removed out of chorions and gently transferred into methylcellulose drop under fish water. Then, detach a few cells from each embryo at the contact

543 points using the pulled glass micropipette and move these two embryos contact each other
544 properly until they fusion together.
545
546 **O-dianisidine staining, Giemsa-staining and Benzidine staining**
547 *smarca5*^{zko1049a} and their sibling embryos at 2 dpf were stained with o-dianisidine staining solution
548 for 15 min in the dark as previously described (Detrich et al., 1995). The blood cells from
549 *smarca5*^{zko1049a} and their sibling embryos at 2 dpf were collected from heart and caudal vein and
550 attached to slides. The dried slides will be stained by Fast Giemsa Stain (Yeasen Biotech Co., Ltd,
551 CAT: 40751ES02) following the standard manufacturer's instructions. The K562 cells were
552 collected and washed once using PBS. Then the cells were suspended using 500 μl PBS.
553 Subsequently, add 10 μl 0.4% benzidine, 1 μl 30% H_2O_2, and 1 μl 5% sodium nitroferricyanide
554 dihydrate and incubate for 3 min, 5 min and 3 min, respectively. Then the cells were attached to
555 slides for further imaging.
556
557 **Chemical treatment**
558 Argatroban (Sigma, A0487), dissolved in DMSO (2 mg/ml), was injected into *smarca5*^{zko1049a} and
559 their sibling embryos at 36 hpf at the dosage of 4 nl/embryo. The control embryos were injected
560 with DMSO alone at the same dosage. Heparin (Sigma, H3393), dissolved in H_2O (2.5 mg/ml),
561 was injected into *smarca5*^{zko1049a} and their sibling embryos at 36 hpf at the dosage of 4 nl/embryo.
562 For aspirin treatment, the *smarca5*^{zko1049a} and sibling embryos at 36 hpf were incubated with
563 aspirin (Sigma, A2093) at the concentration of 5 μg/ml. The *smarca5*^{zko1049a} and sibling embryos
564 at 36 hpf were incubated with Glutathione (Sigma, PHR1359) at the concentration of 0.5 mg/ml.
565
566 **Confocal microscopy**
567 Confocal microscopy was performed using Nikon confocal A1 laser microscope (Nikon) and
568 Andor high speed confocal (dragonfly, Belfast, UK). The embryos were embedded in 1.2% low
569 melting agarose.
570
571 **Generation of transgenic zebrafish**
572 For overexpression experiment, the full length CDS of *keap1a* was cloned into pDestTol2pA2

573 with a *hsp70* promoter and an EGFP reporter by DNA assembly (NEBuilder HiFi DNA Assembly
574 Master Mix, E2621S). The plasmids together with *tol2* mRNA were injected into zebrafish
575 embryos at 1-cell stage to generate Tg (*hsp70*:*flag-keap1a*-EGFP).
576
577 **Short interfering RNAs (siRNAs) and RNA interference**
578 Control and *SMARCA5* siRNAs were synthesized by GenePharma Corporation. The K562 cells
579 were maintained in RPMI-1640 medium supplemented with 10% FBS and stimulated with hemin
580 (Sigma, 51280, 30 μM) for 3 days to induce erythroid differentiation. Then, the hemin-induced
581 K562 cells were transfected with siRNAs using Lipofectamine RNAiMAX Reagent (Invitrogen,
582 13778-030) following the manufacturer's instructions. The detailed sequences are listed in
583 Supplementary file 1C.
584
585 **Western blotting**
586 The western blotting was performed to detect the protein level of SMARCA5 in K562 cells after
587 siRNA transfection. The antibodies used were as followings: anti-Smarca5 antibody (Santa Cruz,
588 H-300: sc-13054), anti-β-Actin antibody (Cell Signaling Technology, 4967).
589
590 **Flow cytometry**
591 The *smarca5*^{zko1049a} and their sibling embryos with Tg (*gata1*:dsRed) background at 2 dpf were
592 collected and washed by Ringers buffer. After digesting into single cell suspension using 0.5%
593 trypsin, the reaction was stopped by adding $CaCl_2$ up to 1 M and fetal calf serum up to 10%. Then
594 the cells were filtered through 300 Mesh nylon cell-strainer to make single cell suspension. The
595 RBCs (*gata1*:dsRed^{+}) were sorted using MoFlo XDP (Beckman Coulter) and collected into PBS
596 containing 1% FBS.
597
598 **RNA-seq**
599 RNA-seq was performed in FACS-purified RBCs from *smarca5*^{zko1049a} and their siblings at 2 dpf.
600 50,000 RBCs were used per sample for RNA-seq experiments. The RNAs of sorted HSPCs were
601 isolated using QIAGEN RNeasy Mini Kit (Cat. No. 74104) following the standard manufacturer's
602 instructions. The mRNA libraries were constructed using NEBNext Ultra RNA Library Prep Kit

603 for Illumina and sequenced under Illumina HiSeq X Ten with pair end 150bp (PE150).

604

605 **Processing of RNA-seq analysis**

606 Raw RNA-seq reads data were trimmed using the fastp (Chen, Zhou, Chen, & Gu, 2018) (v2.4)
607 (parameter: with default parameters), and aligned to "Danio_rerio GRCz10" cDNA reference
608 sequence using the STAR (Dobin et al., 2013) (v 2.7.7a) with the default parameters. Read counts
609 for each gene were quantified as the total number of reads mapping to exons using featureCounts
610 (Liao, Smyth, & Shi, 2014) (subread v1.5.3). DESeq2 (Love, Huber, & Anders, 2014) was applied
611 to perform differential expression analysis with raw counts quantified by featureCounts. We used
612 Benjamini-Hochberg adjusted P-value < 0.05 and log2 fold change > 1 as the threshold for
613 significant difference. Gene set enrichment analysis was performed using *GSEA* function in the
614 clusterProfiler (Yu, Wang, Han, & He, 2012) package (v 3.18.0). Gene set variation analysis was
615 performed by the GSVA (Hanzelmann, Castelo, & Guinney, 2013) package (v 1.38.0). The gene
616 sets we used were exported by the msigdbr package (v 7.2.1). The differences in pathway
617 activities scored between *smarca5*^{zko1049a} and their sibling RBCs were calculated with limma
618 (Ritchie et al., 2015) package (v 3.46.0).

619

620 **Assay for Transposase-Accessible Chromatin with high-throughput sequencing (ATAC-seq)**

621 ATAC-seq was performed in FACS-purified RBCs from *smarca5*^{zko1049a} and their siblings at 2 dpf.
622 50,000 RBCs were used per sample for ATAC-seq library preparation using TruePrep^{TM} DNA
623 Library Prep Kit V2 for Illumina (Vazyme, TD501) as previously described (Ding et al., 2021).
624 Firstly, wash the sorted RBCs using 1xPBST. Then, the cell pellet was lysed using 50 μl cold lysis
625 buffer (10 mM Tris-HCl (pH 7.4), 10 mM NaCl, 3 mM $MgCl_2$ and 0.15% NP-40) for 5 min on ice.
626 Centrifuge and discard the supernatant to get the cell pellet (about 2 μl). Then the transposition
627 reaction system combining 5xTTBL (10 μl), TTE Mix (5 μl) and H_2O (33 μl) was added
628 immediately to the cell pellet and pipetted up and down gently for several times. After the
629 incubation at 37°C for 30 min, the DNA was extracted with chloroform-phenol. After the
630 purification, the DNA was amplified using TruePrep^{TM} DNA Index Kit V2 for Illumina (Vazyme,
631 TD202). After the fragments length purification using VAHTS^{TM} DNA Clean Beads (Vazyme,
632 N411), The DNA libraries are under sequencing under Illumina NovaSeq with pair end 150bp

(PE150).

Processing of ATAC-seq analysis

Raw ATAC-seq reads were trimmed using cutadapt (v 2.4) (parameter: -q 20 -m 20) and mapped to the danRer10 reference genome using Bowtie2 (Langmead & Salzberg, 2012) (v 2.3.4.2) (default parameters). Sorting, removal of PCR duplicates and conversion from SAM to BAM files were performed using SAMtools (H. Li et al., 2009) (v 1.3.1). For quality assessment of ATAC-seq libraries, we applied an R package ATACseqQC (Ou et al., 2018) (v 1.6.4) to check the fragment size distributions, Transcription Start Site (TSS) enrichment scores, and plot heatmaps for nucleosome positions. We employed deepTools2 (Ramirez et al., 2016) (v 2.5.7) to check the reproducibility of the biological replicates and generated bigwig files from BAM output to visualize mapped reads. Peaks were called using MACS2 (Zhang et al., 2008) (v2.1.2) (parameter: --nomodel --nolambda --gsize 1.4e9 --keep-dup all --slocal 10000). Differentially accessible regions were identified using an R package DiffBind (Ross-Innes et al., 2012) (v 2.10.0) with a log2 fold change threshold of 0.5, and Benjamini-Hochberg adjusted P-value < 0.1. Peak annotation was performed by an R package ChIPseeker (Yu, Wang, & He, 2015) (v 1.18.0). We identified the enriched de novo motifs across the whole genomic regions using the findMotifsGenome.pl function of HOMER (Heinz et al., 2010) (parameter: -size 500 -len 8,10,12 -mask -dumpFasta).

Transmission electron microscopy

The tail region of *smarca5*^{zko1049a} and their siblings at 2 dpf were fixed with 2.5% (vol/vol) glutaraldehyde and 2% paraformaldehyde in phosphate buffer (PB) (0.1 M, pH 7.4). After washing with PB for four times, the tissues were immersed in 1% (wt/vol) OsO_4 and 1.5% (wt/vol) potassium ferricyanide aqueous solution at 4°C for 1 hour. After washing, the tissues were incubated in filtered 1% thiocarbohydrazide (TCH) aqueous solution (Sigma-Aldrich) at room temperature for 30 min, followed by 1% unbuffered OsO_4 aqueous solution at 4°C for 1 hour and 1% UA aqueous solution at room temperature for 2 hours. The tissues were dehydrated through graded alcohol (30%, 50%, 70%, 80%, 90%, 100%, 100%, 10 min each, at 4°C). Then, transfer the tissues into pure acetone for 10 min (twice). Tissues were infiltrated in graded mixtures of

acetone and SPI-PON812 resin (21 ml SPI-PON812, 13 ml DDSA and 11ml NMA) (3:1, 1:1, 1:3), then transfer the tissues into pure resin. Finally, the tissues were embedded in pure resin with 1.5% BDMA and polymerized at 45°C for 12 hours, followed by at 60°C for 48 hours. The ultrathin sections (70 nm thick) were sectioned with microtome (Leica EM UC6), and examined by a transmission electron microscope (FEI Tecnai Spirit120kV).

Image Analysis

Raw image data were processed using ImageJ, photoshop CC 2018 and Adobe Illustrator CC 2018.

Statistical Analysis

All of the statistical analysis was performed for at least three independent biological repeats. GraphPad Prism 6 was used to analyze the data. Data are mean ± s.d. *P* values calculated by two-tailed unpaired Student's *t*-test were used to indicate the significance if not clarified in figure legends.

DATA AVAILABILITY

The accession number for the sequencing raw data in this paper is BioProject: PRJNA716463. Source data of supplemental Figure 6D was provided, including the original files of the full raw unedited blots (supplemental Figure 6-source data 2 and 4) and figures with the uncropped blots with the relevant bands clearly labelled (supplemental Figure 6-source data 1 and 3).

Acknowledgments

We thank Lihong Shi and Jun Peng for critical reading of this paper. We are grateful to Xixia Li, and Xueke Tan for helping with electron microscopy sample preparation and taking TEM images at the Center for Biological Imaging (CBI), Institute of Biophysics, Chinese Academy of Science. This work was supported by grants from the National Key Research and Development Program of China (2018YFA0800200), the Strategic Priority Research Program of the Chinese Academy of Sciences, China (XDA16010207), the National Natural Science Foundation of China (31830061, 31425016, and 81530004), and the State Key Laboratory of Membrane Biology, China.

693

694 **Authorship Contributions**

695 Y.D. performed most of the experiments; Y.L. performed the bioinformatics analysis; Y.D., Y.L.,
696 Q.Z., and F.L. conceived the project, analyzed the data, and wrote the paper. All authors read and
697 approved the final manuscript.

698

699 **Conflict of Interest Disclosures**

700 The authors declare no competing interests.

701

References

Akin-Bali, D. F., Eroglu, T., Ilk, S., Egin, Y., & Kankilic, T. (2020). Evaluation of the role of Nrf2/Keap1 pathway-associated novel mutations and gene expression on antioxidant status in patients with deep vein thrombosis. *Exp Ther Med, 20*(2), 868-881. doi:10.3892/etm.2020.8790

Bertrand, J. Y., Chi, N. C., Santoso, B., Teng, S. T., Stainier, D. Y. R., & Traver, D. (2010). Haematopoietic stem cells derive directly from aortic endothelium during development. *Nature, 464*(7285), 108-U120. doi:10.1038/nature08738

Bultman, S. J., Gebuhr, T. C., & Magnuson, T. (2005). A Brg1 mutation that uncouples ATPase activity from chromatin remodeling reveals an essential role for SWI/SNF-related complexes in beta-globin expression and erythroid development. *Genes Dev, 19*(23), 2849-2861. doi:10.1101/gad.1364105

Chen, S., Zhou, Y., Chen, Y., & Gu, J. (2018). fastp: an ultra-fast all-in-one FASTQ preprocessor. *Bioinformatics, 34*(17), i884-i890. doi:10.1093/bioinformatics/bty560

Clapier, C. R., Iwasa, J., Cairns, B. R., & Peterson, C. L. (2017). Mechanisms of action and regulation of ATP-dependent chromatin-remodelling complexes. *Nat Rev Mol Cell Biol, 18*(7), 407-422. doi:10.1038/nrm.2017.26

Demy, D. L., Ranta, Z., Giorgi, J. M., Gonzalez, M., Herbomel, P., & Kissa, K. (2013). Generating parabiotic zebrafish embryos for cell migration and homing studies. *Nat Methods, 10*(3), 256-258. doi:10.1038/nmeth.2362

Detrich, H. W., 3rd, Kieran, M. W., Chan, F. Y., Barone, L. M., Yee, K., Rundstadler, J. A., Pratt, S., Ransom, D., & Zon, L. I. (1995). Intraembryonic hematopoietic cell migration

during vertebrate development. *Proc Natl Acad Sci U S A, 92*(23), 10713-10717. doi:10.1073/pnas.92.23.10713

Diaz, J. A., Saha, P., Cooley, B., Palmer, O. R., Grover, S. P., Mackman, N., Wakefield, T. W., Henke, P. K., Smith, A., & Lal, B. K. (2019). Choosing a mouse model of venous thrombosis: a consensus assessment of utility and application. *J Thromb Haemost, 17*(4), 699-707. doi:10.1111/jth.14413

Ding, Y., Wang, W., Ma, D., Liang, G., Kang, Z., Xue, Y., Zhang, Y., Wang, L., Heng, J., Zhang, Y., & Liu, F. (2021). Smarca5-mediated epigenetic programming facilitates fetal HSPC development in vertebrates. *Blood, 137*(2), 190-202. doi:10.1182/blood.2020005219

Dluhosova, M., Curik, N., Vargova, J., Jonasova, A., Zikmund, T., & Stopka, T. (2014). Epigenetic control of SPI1 gene by CTCF and ISWI ATPase SMARCA5. *Plos One, 9*(2), e87448. doi:10.1371/journal.pone.0087448

Dobin, A., Davis, C. A., Schlesinger, F., Drenkow, J., Zaleski, C., Jha, S., Batut, P., Chaisson, M., & Gingeras, T. R. (2013). STAR: ultrafast universal RNA-seq aligner. *Bioinformatics, 29*(1), 15-21. doi:10.1093/bioinformatics/bts635

Gao, Z., Huang, Z., Olivey, H. E., Gurbuxani, S., Crispino, J. D., & Svensson, E. C. (2010). FOG-1-mediated recruitment of NuRD is required for cell lineage re-enforcement during haematopoiesis. *Embo Journal, 29*(2), 457-468. doi:10.1038/emboj.2009.368

Garcia-Santos, D., Schranzhofer, M., Horvathova, M., Jaberi, M. M., Bogo Chies, J. A., Sheftel, A. D., & Ponka, P. (2014). Heme oxygenase 1 is expressed in murine erythroid cells where it controls the level of regulatory heme. *Blood, 123*(14), 2269-2277. doi:10.1182/blood-2013-04-496760

746 Gregory, G. D., Miccio, A., Bersenev, A., Wang, Y., Hong, W., Zhang, Z., Poncz, M., Tong, W.,
747 & Blobel, G. A. (2010). FOG1 requires NuRD to promote hematopoiesis and maintain
748 lineage fidelity within the megakaryocytic-erythroid compartment. *Blood, 115*(11),
749 2156-2166. doi:10.1182/blood-2009-10-251280
750 Gregory, M., Hanumanthaiah, R., & Jagadeeswaran, P. (2002). Genetic analysis of
751 hemostasis and thrombosis using vascular occlusion. *Blood Cells Mol Dis, 29*(3),
752 286-295. doi:10.1006/bcmd.2002.0568
753 Griffin, C. T., Brennan, J., & Magnuson, T. (2008). The chromatin-remodeling enzyme BRG1
754 plays an essential role in primitive erythropoiesis and vascular development.
755 *Development, 135*(3), 493-500. doi:10.1242/dev.010090
756 Grover, S. P., & Mackman, N. (2019). Intrinsic Pathway of Coagulation and Thrombosis.
757 *Arterioscler Thromb Vasc Biol, 39*(3), 331-338. doi:10.1161/ATVBAHA.118.312130
758 Hagedorn, E. J., Cillis, J. L., Curley, C. R., Patch, T. C., Li, B., Blaser, B. W., Riquelme, R., Zon,
759 L. I., & Shah, D. I. (2016). Generation of Parabiotic Zebrafish Embryos by Surgical
760 Fusion of Developing Blastulae. *J Vis Exp*(112). doi:10.3791/54168
761 Hanumanthaiah, R., Day, K., & Jagadeeswaran, P. (2002). Comprehensive analysis of blood
762 coagulation pathways in teleostei: evolution of coagulation factor genes and
763 identification of zebrafish factor VIIi. *Blood Cells Mol Dis, 29*(1), 57-68.
764 doi:10.1006/bcmd.2002.0534
765 Hanzelmann, S., Castelo, R., & Guinney, J. (2013). GSVA: gene set variation analysis for
766 microarray and RNA-seq data. *BMC Bioinformatics, 14*, 7.
767 doi:10.1186/1471-2105-14-7

768 Hassannia, B., Vandenabeele, P., & Vanden Berghe, T. (2019). Targeting Ferroptosis to Iron
769 Out Cancer. *Cancer Cell, 35*(6), 830-849. doi:10.1016/j.ccell.2019.04.002
770 Heinz, S., Benner, C., Spann, N., Bertolino, E., Lin, Y. C., Laslo, P., Cheng, J. X., Murre, C.,
771 Singh, H., & Glass, C. K. (2010). Simple combinations of lineage-determining
772 transcription factors prime cis-regulatory elements required for macrophage and B cell
773 identities. *Mol Cell, 38*(4), 576-589. doi:10.1016/j.molcel.2010.05.004
774 Hewitt, K. J., Sanalkumar, R., Johnson, K. D., Keles, S., & Bresnick, E. H. (2014). Epigenetic
775 and genetic mechanisms in red cell biology. *Curr Opin Hematol, 21*(3), 155-164.
776 doi:10.1097/MOH.0000000000000034
777 Itoh, K., Chiba, T., Takahashi, S., Ishii, T., Igarashi, K., Katoh, Y., Oyake, T., Hayashi, N.,
778 Satoh, K., Hatayama, I., Yamamoto, M., & Nabeshima, Y. (1997). An Nrf2/small Maf
779 heterodimer mediates the induction of phase II detoxifying enzyme genes through
780 antioxidant response elements. *Biochem Biophys Res Commun, 236*(2), 313-322.
781 doi:10.1006/bbrc.1997.6943
782 Itoh, K., Wakabayashi, N., Katoh, Y., Ishii, T., Igarashi, K., Engel, J. D., & Yamamoto, M.
783 (1999). Keap1 represses nuclear activation of antioxidant responsive elements by
784 Nrf2 through binding to the amino-terminal Neh2 domain. *Genes Dev, 13*(1), 76-86.
785 doi:10.1101/gad.13.1.76
786 Jagadeeswaran, P., Sheehan, J. P., Craig, F. E., & Troyer, D. (1999). Identification and
787 characterization of zebrafish thrombocytes. *Br J Haematol, 107*(4), 731-738.
788 doi:10.1046/j.1365-2141.1999.01763.x
789 Kato, G. J., Piel, F. B., Reid, C. D., Gaston, M. H., Ohene-Frempong, K., Krishnamurti, L.,

790 Smith, W. R., Panepinto, J. A., Weatherall, D. J., Costa, F. F., & Vichinsky, E. P.
791 (2018). Sickle cell disease. *Nat Rev Dis Primers, 4*, 18010. doi:10.1038/nrdp.2018.10
792 Langmead, B., & Salzberg, S. L. (2012). Fast gapped-read alignment with Bowtie 2. *Nat*
793 *Methods, 9*(4), 357-359. doi:10.1038/nmeth.1923
794 Lewerenz, J., Ates, G., Methner, A., Conrad, M., & Maher, P. (2018).
795 Oxytosis/Ferroptosis-(Re-) Emerging Roles for Oxidative Stress-Dependent
796 Non-apoptotic Cell Death in Diseases of the Central Nervous System. *Front Neurosci,*
797 *12*, 214. doi:10.3389/fnins.2018.00214
798 Li, H., Handsaker, B., Wysoker, A., Fennell, T., Ruan, J., Homer, N., Marth, G., Abecasis, G.,
799 Durbin, R., & Genome Project Data Processing, Subgroup. (2009). The Sequence
800 Alignment/Map format and SAMtools. *Bioinformatics, 25*(16), 2078-2079.
801 doi:10.1093/bioinformatics/btp352
802 Li, L., Yan, B., Shi, Y. Q., Zhang, W. Q., & Wen, Z. L. (2012). Live Imaging Reveals Differing
803 Roles of Macrophages and Neutrophils during Zebrafish Tail Fin Regeneration.
804 *Journal of Biological Chemistry, 287*(30), 25353-25360. doi:10.1074/jbc.M112.349126
805 Liao, Y., Smyth, G. K., & Shi, W. (2014). featureCounts: an efficient general purpose program
806 for assigning sequence reads to genomic features. *Bioinformatics, 30*(7), 923-930.
807 doi:10.1093/bioinformatics/btt656
808 Lin, H. F., Traver, D., Zhu, H., Dooley, K., Paw, B. H., Zen, L. I., & Handin, R. I. (2005).
809 Analysis of thrombocyte development in CD41-GFP transgenic zebrafish. *Blood,*
810 *106*(12), 3803-3810. doi:10.1182/blood-2005-01-0179
811 Liu, Y., Kretz, C. A., Maeder, M. L., Richter, C. E., Tsao, P., Vo, A. H., Huarng, M. C., Rode, T.,

812 Hu, Z., Mehra, R., Olson, S. T., Joung, J. K., & Shavit, J. A. (2014). Targeted
813 mutagenesis of zebrafish antithrombin III triggers disseminated intravascular
814 coagulation and thrombosis, revealing insight into function. *Blood, 124*(1), 142-150.
815 doi:10.1182/blood-2014-03-561027
816 Love, M. I., Huber, W., & Anders, S. (2014). Moderated estimation of fold change and
817 dispersion for RNA-seq data with DESeq2. *Genome Biol, 15*(12), 550.
818 doi:10.1186/s13059-014-0550-8
819 Mackman, N. (2008). Triggers, targets and treatments for thrombosis. *Nature, 451*(7181),
820 914-918. doi:10.1038/nature06797
821 Mackman, N., Bergmeier, W., Stouffer, G. A., & Weitz, J. I. (2020). Therapeutic strategies for
822 thrombosis: new targets and approaches. *Nat Rev Drug Discov, 19*(5), 333-352.
823 doi:10.1038/s41573-020-0061-0
824 Miccio, A., & Blobel, G. A. (2010). Role of the GATA-1/FOG-1/NuRD pathway in the
825 expression of human beta-like globin genes. *Mol Cell Biol, 30*(14), 3460-3470.
826 doi:10.1128/MCB.00001-10
827 Murakami, S., Shimizu, R., Romeo, P. H., Yamamoto, M., & Motohashi, H. (2014). Keap1-Nrf2
828 system regulates cell fate determination of hematopoietic stem cells. *Genes Cells,*
829 *19*(3), 239-253. doi:10.1111/gtc.12126
830 Ou, J., Liu, H., Yu, J., Kelliher, M. A., Castilla, L. H., Lawson, N. D., & Zhu, L. J. (2018).
831 ATACseqQC: a Bioconductor package for post-alignment quality assessment of
832 ATAC-seq data. *BMC Genomics, 19*(1), 169. doi:10.1186/s12864-018-4559-3
833 Ramirez, F., Ryan, D. P., Gruning, B., Bhardwaj, V., Kilpert, F., Richter, A. S., Heyne, S.,

834 Dundar, F., & Manke, T. (2016). deepTools2: a next generation web server for
835 deep-sequencing data analysis. *Nucleic Acids Res, 44*(W1), W160-165.
836 doi:10.1093/nar/gkw257
837 Renshaw, S. A., Loynes, C. A., Trushell, D. M. I., Elworthy, S., Ingham, P. W., & Whyte, M. K.
838 B. (2006). A transgenic zebrafish model of neutrophilic inflammation. *Blood, 108*(13),
839 3976-3978. doi:10.1182/blood-2006-05-024075
840 Ritchie, M. E., Phipson, B., Wu, D., Hu, Y., Law, C. W., Shi, W., & Smyth, G. K. (2015). limma
841 powers differential expression analyses for RNA-sequencing and microarray studies.
842 *Nucleic Acids Res, 43*(7), e47. doi:10.1093/nar/gkv007
843 Rodriguez, P., Bonte, E., Krijgsveld, J., Kolodziej, K. E., Guyot, B., Heck, A. J., Vyas, P., de
844 Boer, E., Grosveld, F., & Strouboulis, J. (2005). GATA-1 forms distinct activating and
845 repressive complexes in erythroid cells. *Embo Journal, 24*(13), 2354-2366.
846 doi:10.1038/sj.emboj.7600702
847 Rodriguez-Garcia, R., Lopez-Montero, I., Mell, M., Egea, G., Gov, N. S., & Monroy, F. (2016).
848 Direct Cytoskeleton Forces Cause Membrane Softening in Red Blood Cells. *Biophys J,*
849 *111*(5), 1101. doi:10.1016/j.bpj.2016.08.022
850 Ross-Innes, C. S., Stark, R., Teschendorff, A. E., Holmes, K. A., Ali, H. R., Dunning, M. J.,
851 Brown, G. D., Gojis, O., Ellis, I. O., Green, A. R., Ali, S., Chin, S. F., Palmieri, C.,
852 Caldas, C., & Carroll, J. S. (2012). Differential oestrogen receptor binding is
853 associated with clinical outcome in breast cancer. *Nature, 481*(7381), 389-393.
854 doi:10.1038/nature10730
855 Roumenina, L. T., Rayes, J., Lacroix-Desmazes, S., & Dimitrov, J. D. (2016). Heme:

Modulator of Plasma Systems in Hemolytic Diseases. *Trends Mol Med, 22*(3), 200-213. doi:10.1016/j.molmed.2016.01.004

Sheehan, J., Templer, M., Gregory, M., Hanumanthaiah, R., Troyer, D., Phan, T., Thankavel, B., & Jagadeeswaran, P. (2001). Demonstration of the extrinsic coagulation pathway in teleostei: identification of zebrafish coagulation factor VII. *Proc Natl Acad Sci U S A, 98*(15), 8768-8773. doi:10.1073/pnas.131109398

Traver, D., Paw, B. H., Poss, K. D., Penberthy, W. T., Lin, S., & Zon, L. I. (2003). Transplantation and in vivo imaging of multilineage engraftment in zebrafish bloodless mutants. *Nature Immunology, 4*(12), 1238-1246. doi:10.1038/ni1007

Wang, L., Zhang, P. P., Wei, Y. L., Gao, Y., Patient, R., & Liu, F. (2011). A blood flow-dependent klf2a-NO signaling cascade is required for stabilization of hematopoietic stem cell programming in zebrafish embryos. *Blood, 118*(15), 4102-4110. doi:10.1182/blood-2011-05-353235

Weisel, J. W., & Litvinov, R. I. (2019). Red blood cells: the forgotten player in hemostasis and thrombosis. *J Thromb Haemost, 17*(2), 271-282. doi:10.1111/jth.14360

Wendelboe, A. M., & Raskob, G. E. (2016). Global Burden of Thrombosis: Epidemiologic Aspects. *Circ Res, 118*(9), 1340-1347. doi:10.1161/CIRCRESAHA.115.306841

Wolberg, A. S., Rosendaal, F. R., Weitz, J. I., Jaffer, I. H., Agnelli, G., Baglin, T., & Mackman, N. (2015). Venous thrombosis. *Nat Rev Dis Primers, 1*, 15006. doi:10.1038/nrdp.2015.6

Yu, G., Wang, L. G., Han, Y., & He, Q. Y. (2012). clusterProfiler: an R package for comparing biological themes among gene clusters. *OMICS, 16*(5), 284-287.

878 doi:10.1089/omi.2011.0118

879 Yu, G., Wang, L. G., & He, Q. Y. (2015). ChIPseeker: an R/Bioconductor package for ChIP
880 peak annotation, comparison and visualization. *Bioinformatics, 31*(14), 2382-2383.
881 doi:10.1093/bioinformatics/btv145

882 Zapilko, V., Fish, R. J., Garcia, A., Reny, J. L., Dunoyer-Geindre, S., Lecompte, T.,
883 Neerman-Arbez, M., & Fontana, P. (2020). MicroRNA-126 is a regulator of
884 platelet-supported thrombin generation. *Platelets, 31*(6), 746-755.
885 doi:10.1080/09537104.2020.1775804

886 Zhang, Y., Liu, T., Meyer, C. A., Eeckhoute, J., Johnson, D. S., Bernstein, B. E., Nusbaum, C.,
887 Myers, R. M., Brown, M., Li, W., & Liu, X. S. (2008). Model-based analysis of
888 ChIP-Seq (MACS). *Genome Biol, 9*(9), R137. doi:10.1186/gb-2008-9-9-r137

889 Zhu, X. Y., Liu, H. C., Guo, S. Y., Xia, B., Song, R. S., Lao, Q. C., Xuan, Y. X., & Li, C. Q.
890 (2016). A Zebrafish Thrombosis Model for Assessing Antithrombotic Drugs. *Zebrafish,*
891 *13*(4), 335-344. doi:10.1089/zeb.2016.1263

892

Figure S1

A

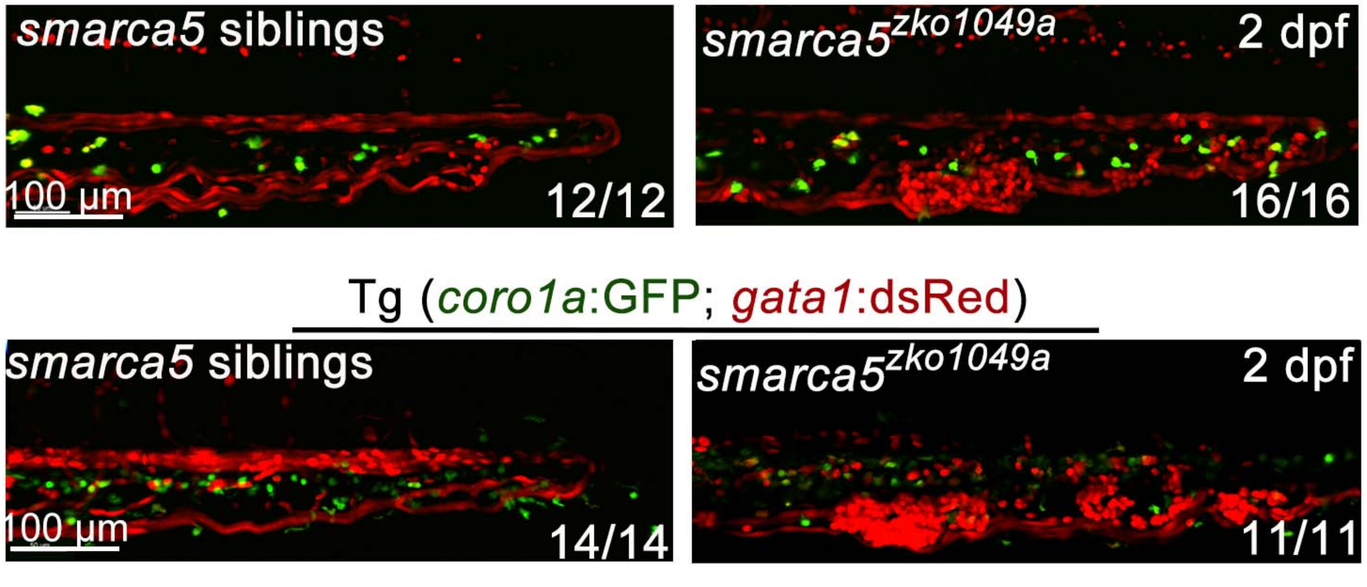

B

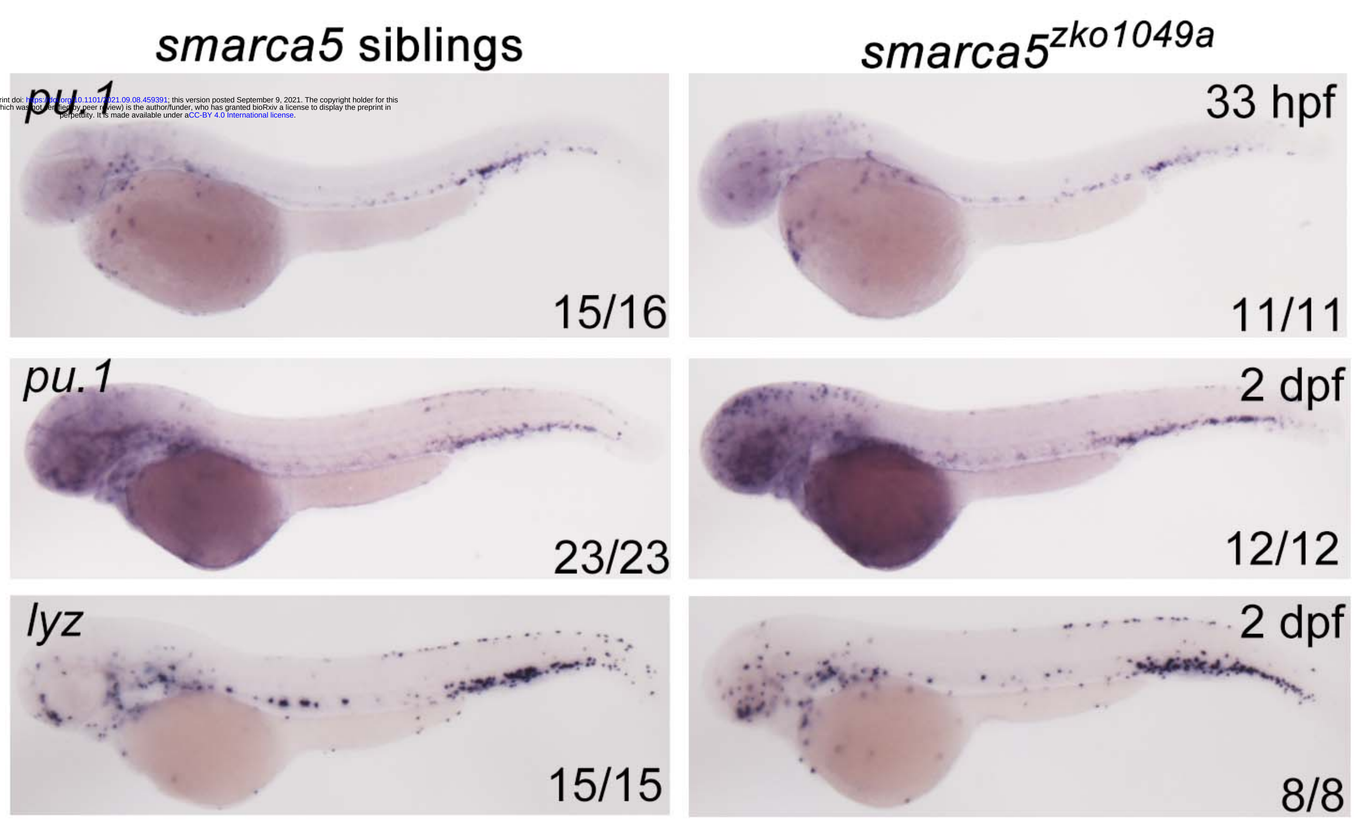

C

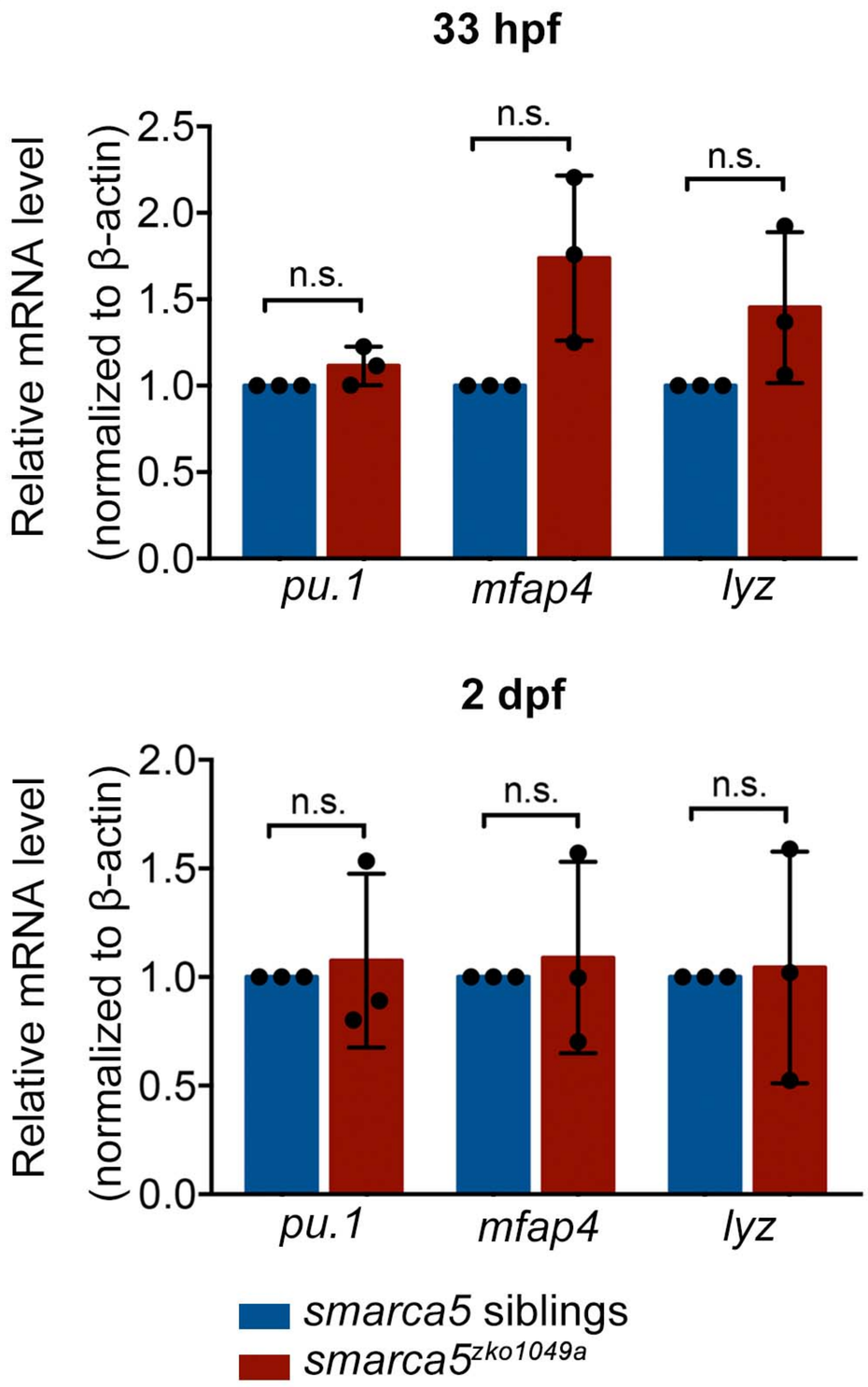

Figure S2

A

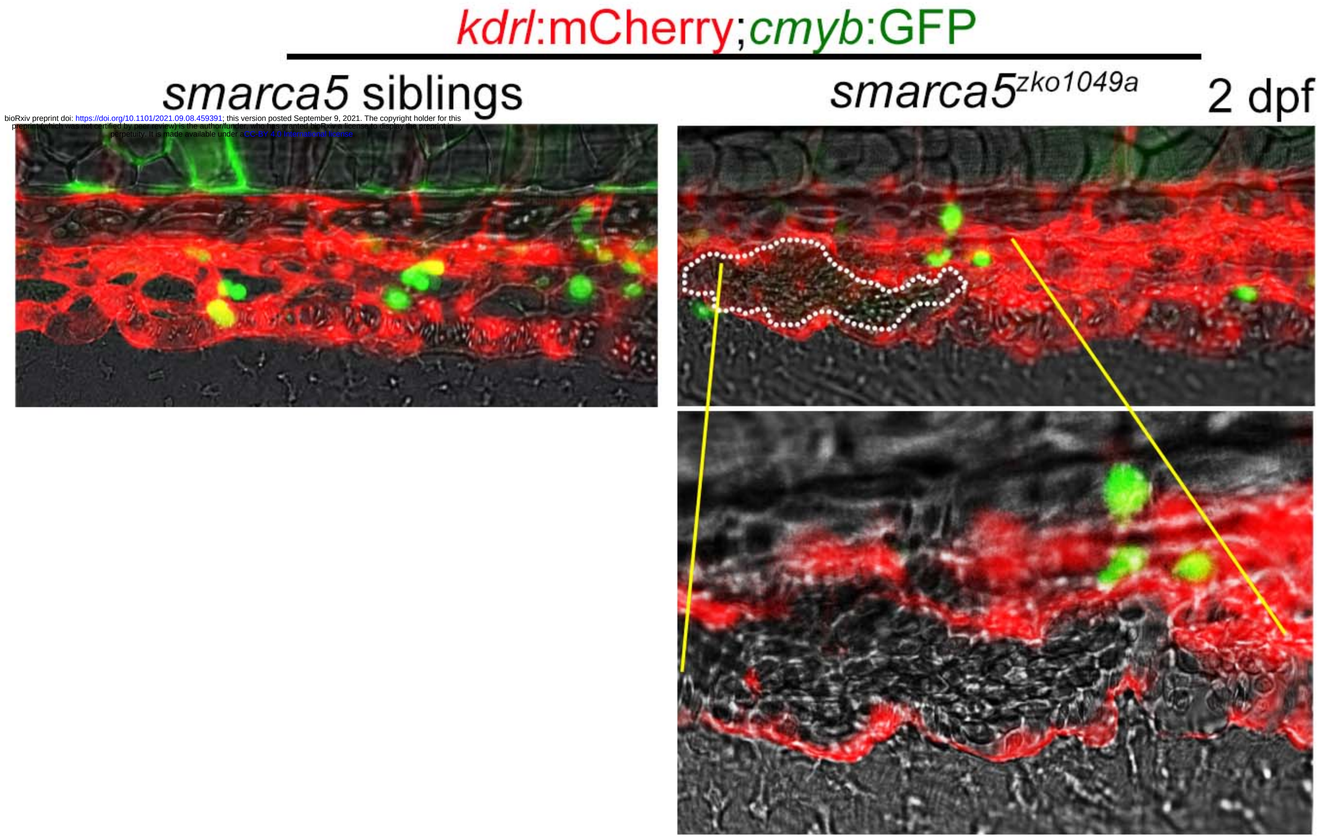

B

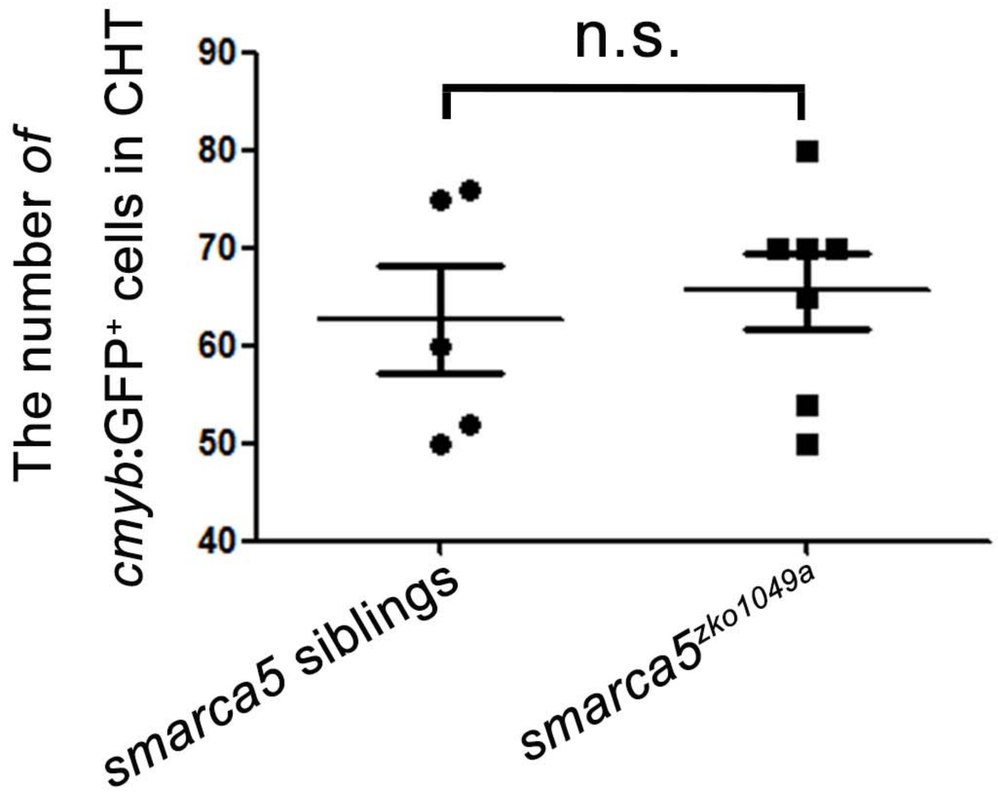

Figure S3

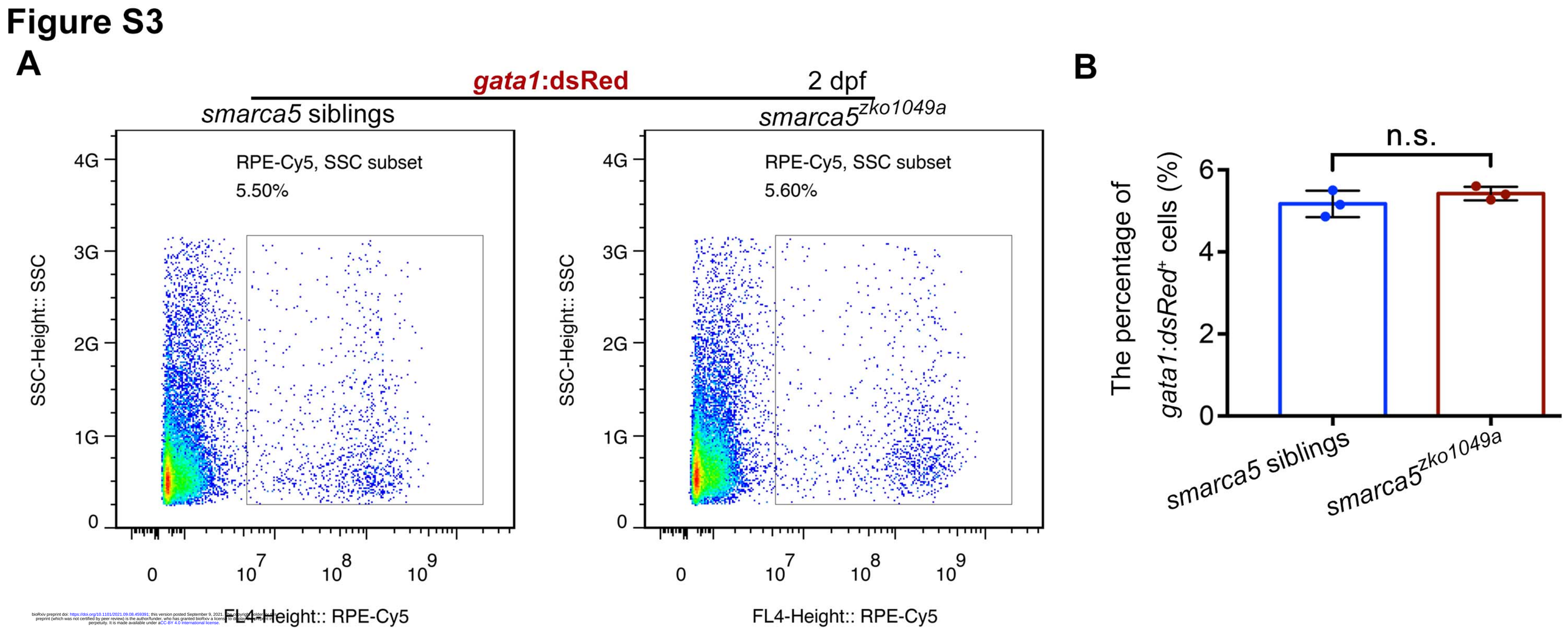

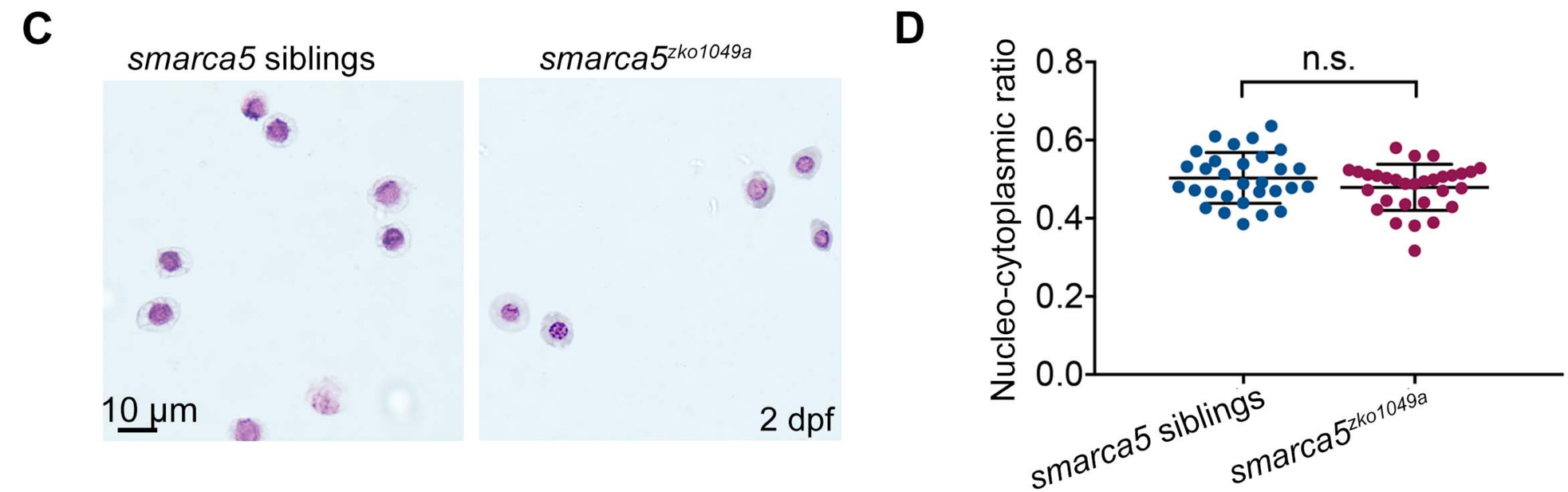

Figure S4

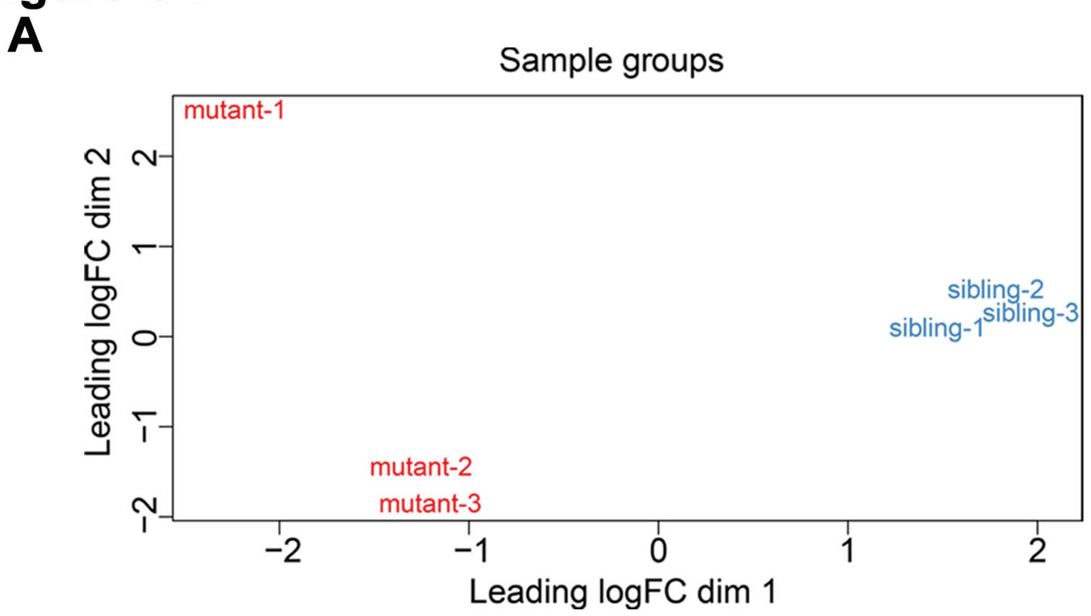
A
Sample groups
mutant-1
mutant-2
mutant-3
sibling-1
sibling-2
sibling-3
Leading logFC dim 2
Leading logFC dim 1

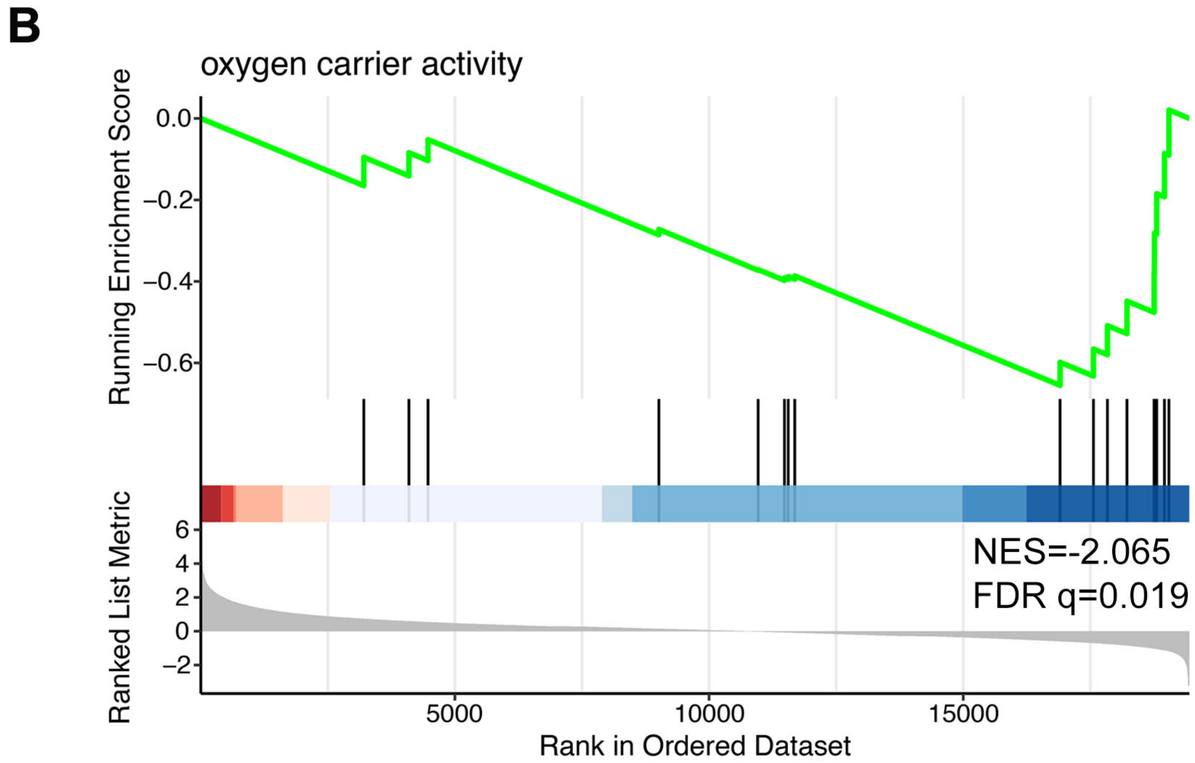
B
oxygen carrier activity
Running Enrichment Score
Ranked List Metric
NES=-2.065
FDR q=0.019
Rank in Ordered Dataset

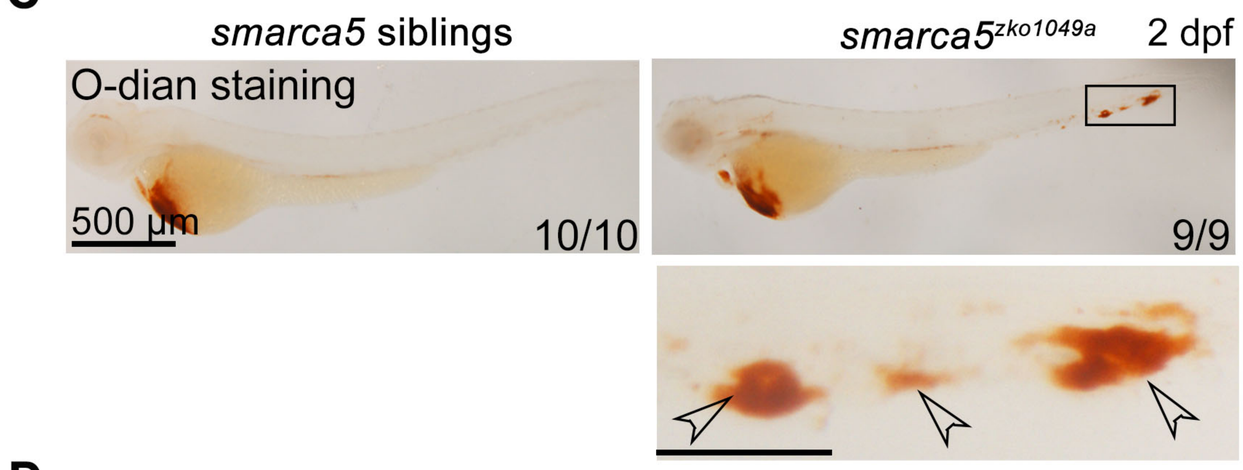
C
smarca5 siblings
smarca5zko1049a
2 dpf
O-dian staining
500 μm
10/10
9/9

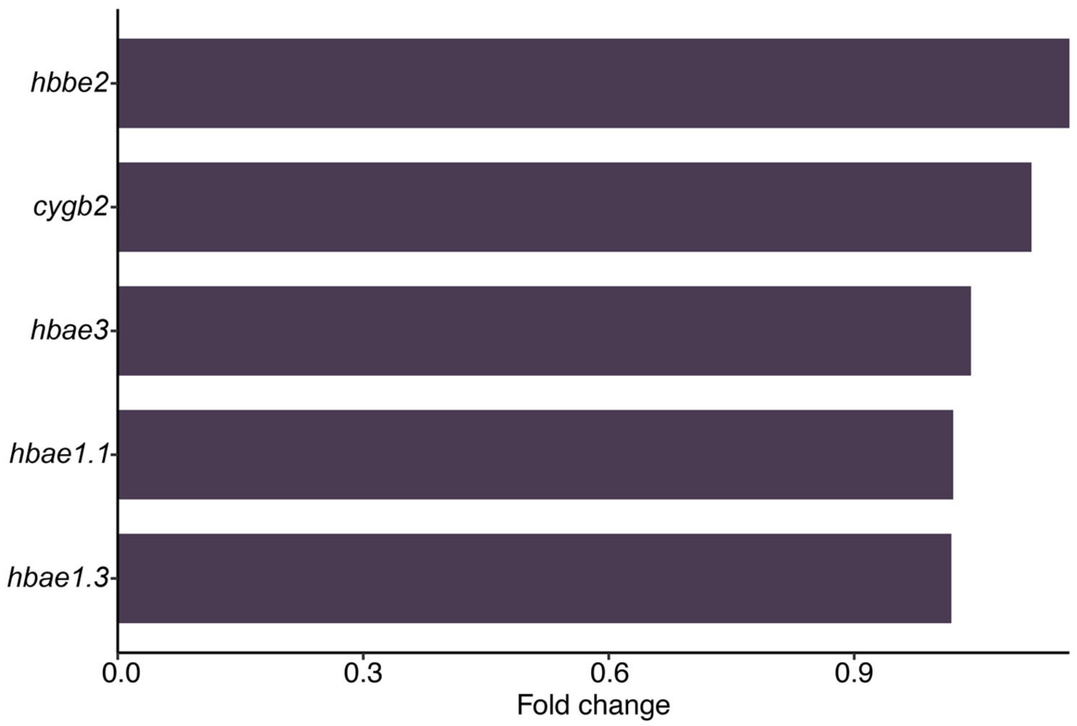
hbbe2
cygb2
hbae3
hbae1.1
hbae1.3
Fold change

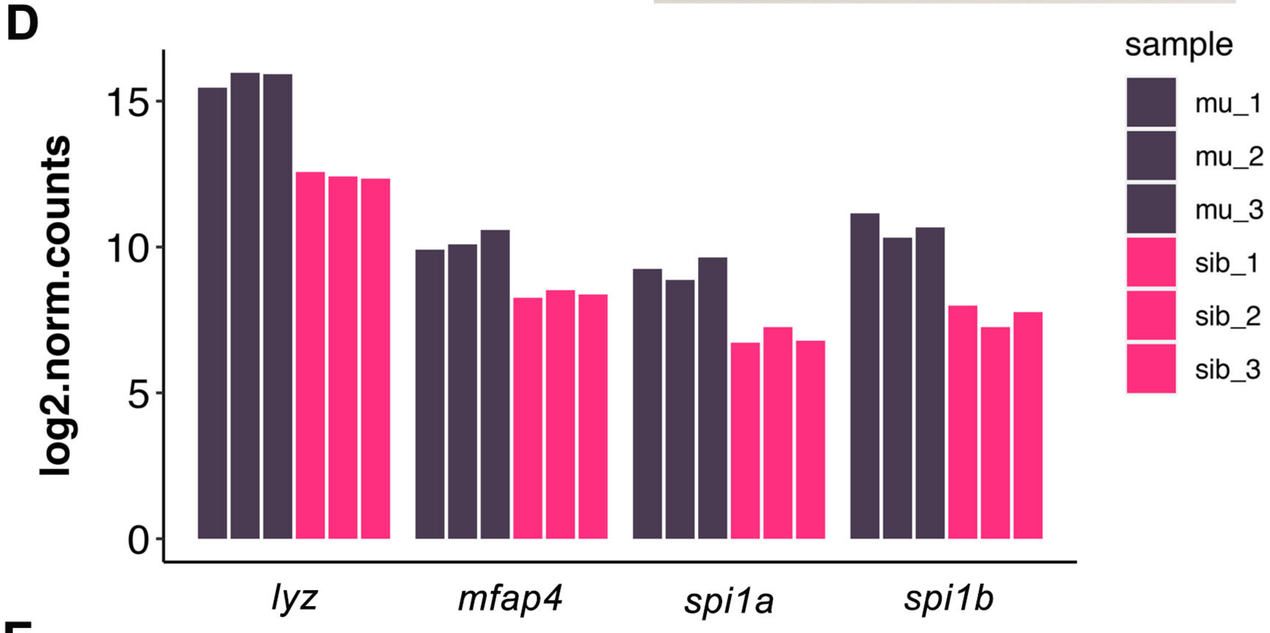
D
log2.norm.counts
sample
mu_1
mu_2
mu_3
sib_1
sib_2
sib_3
lyz
mfap4
spi1a
spi1b

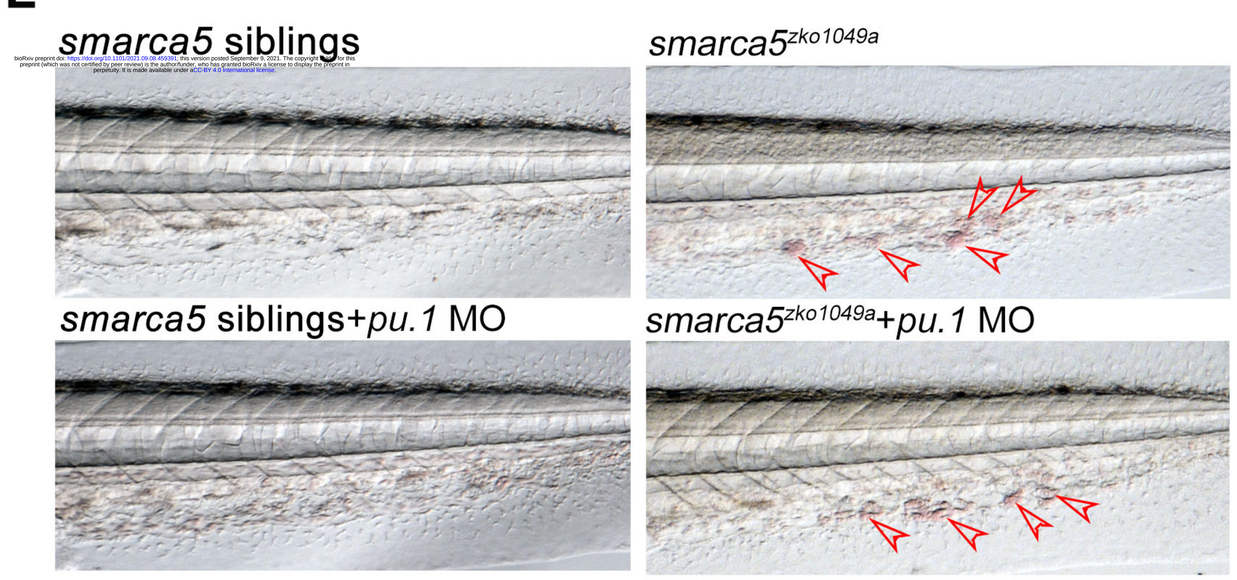
E
smarca5 siblings
smarca5zko1049a
smarca5 siblings+pu.1 MO
smarca5zko1049a+pu.1 MO

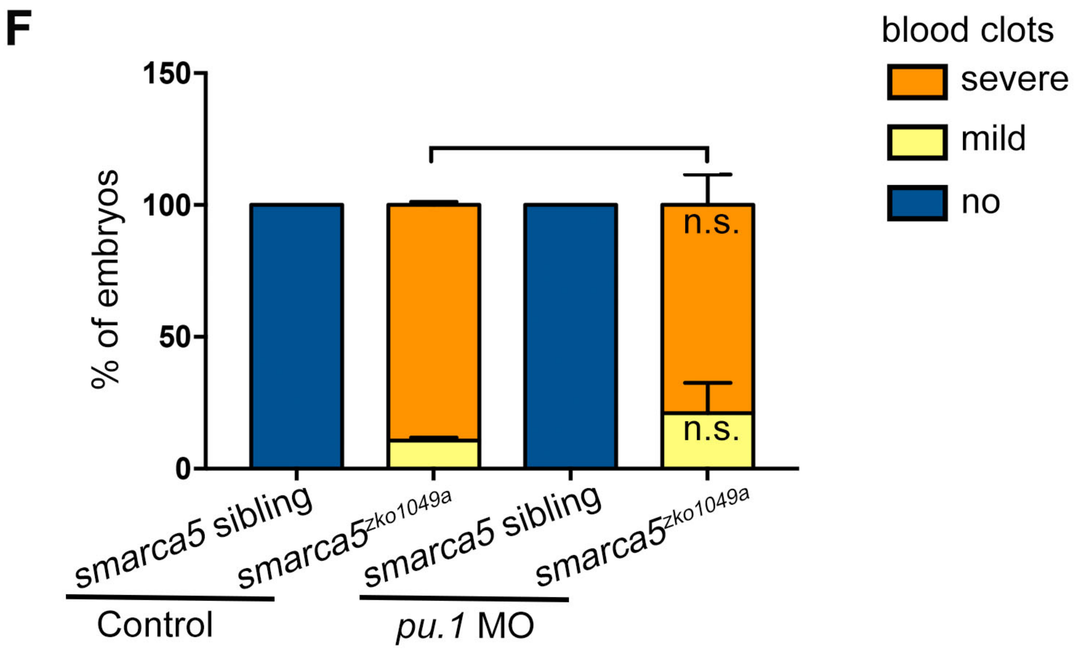
F
blood clots
severe
mild
no
% of embryos
n.s.
n.s.
smarca5 sibling
smarca5zko1049a
smarca5 sibling
smarca5zko1049a
Control
pu.1 MO

Figure S5

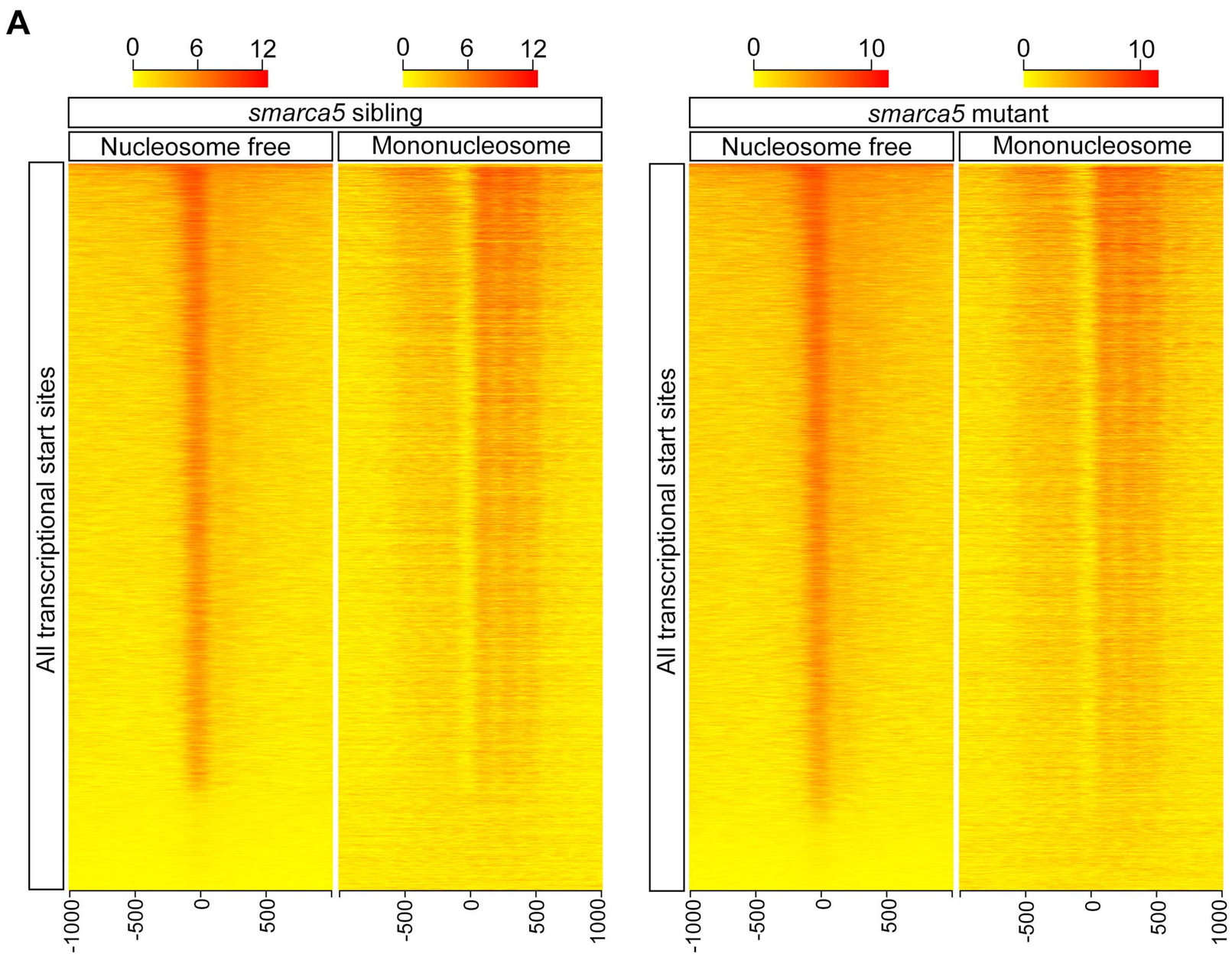

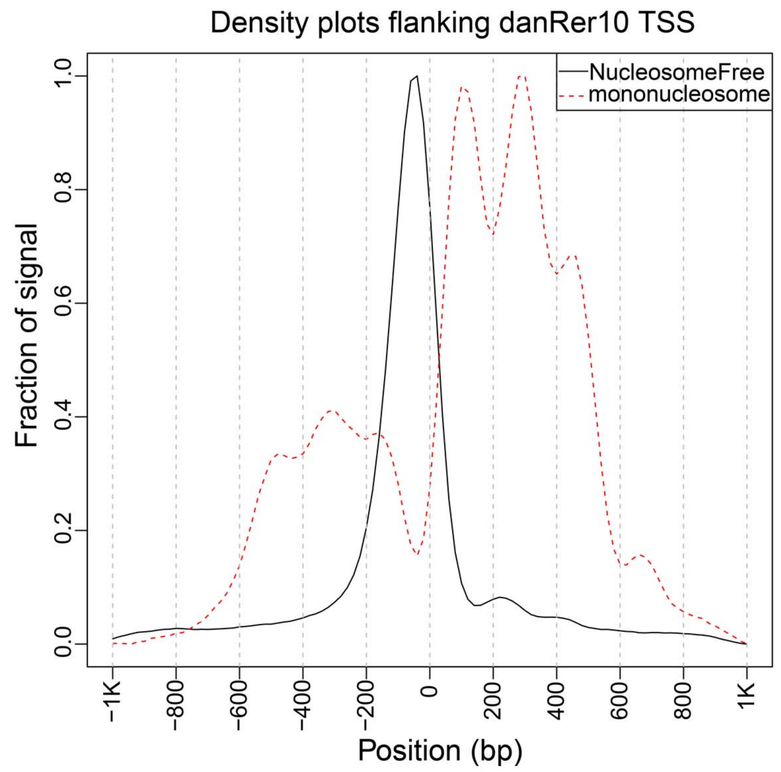

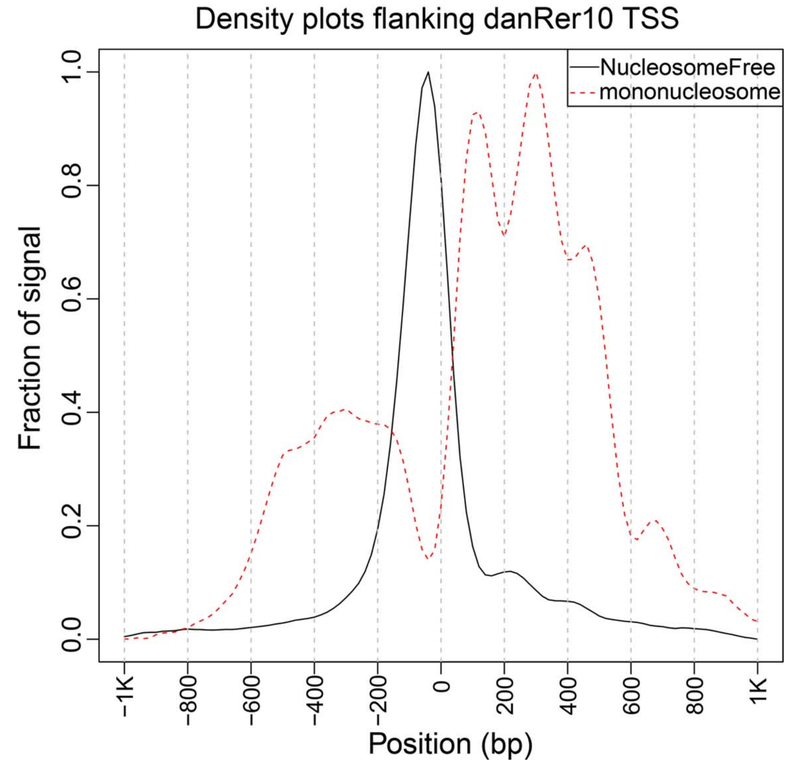

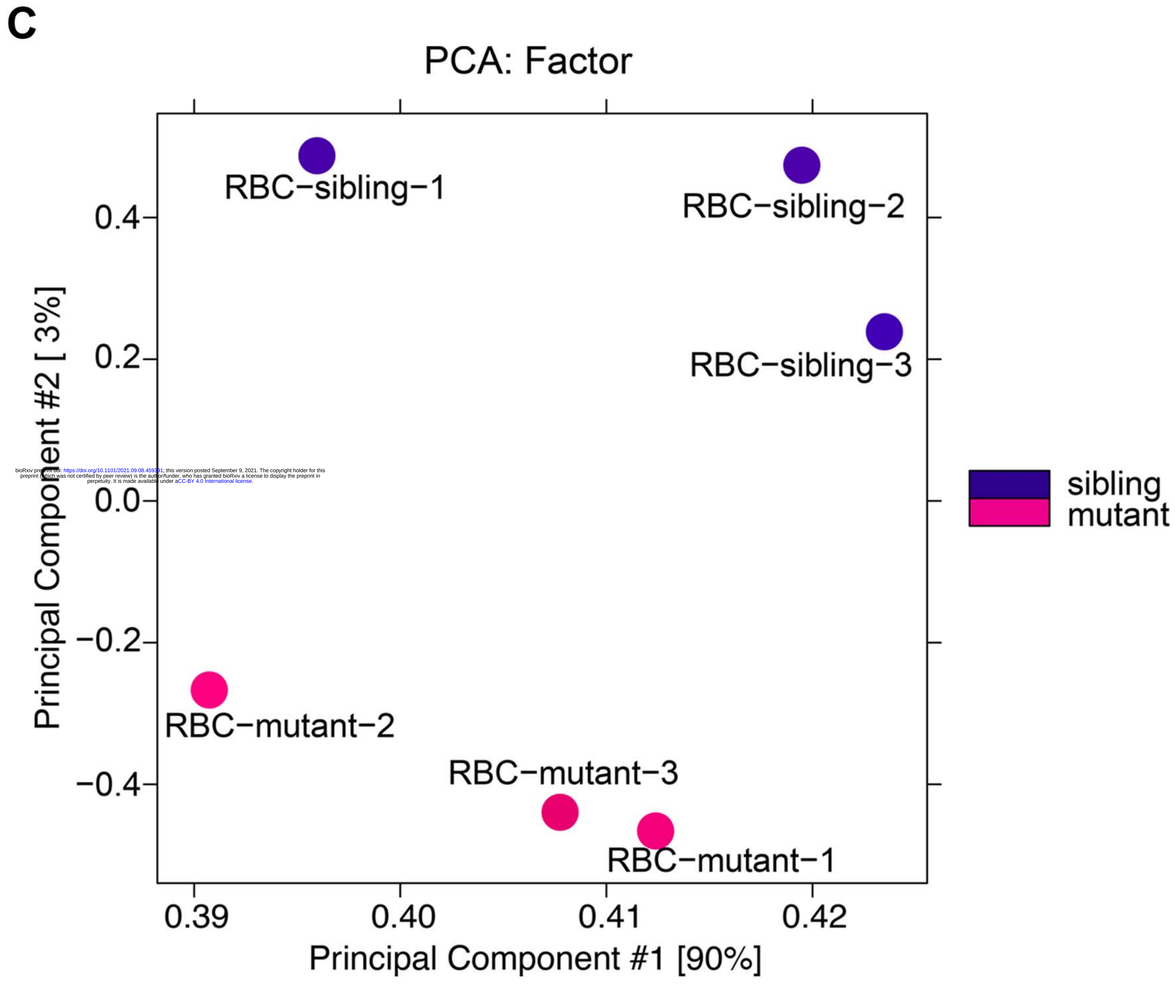

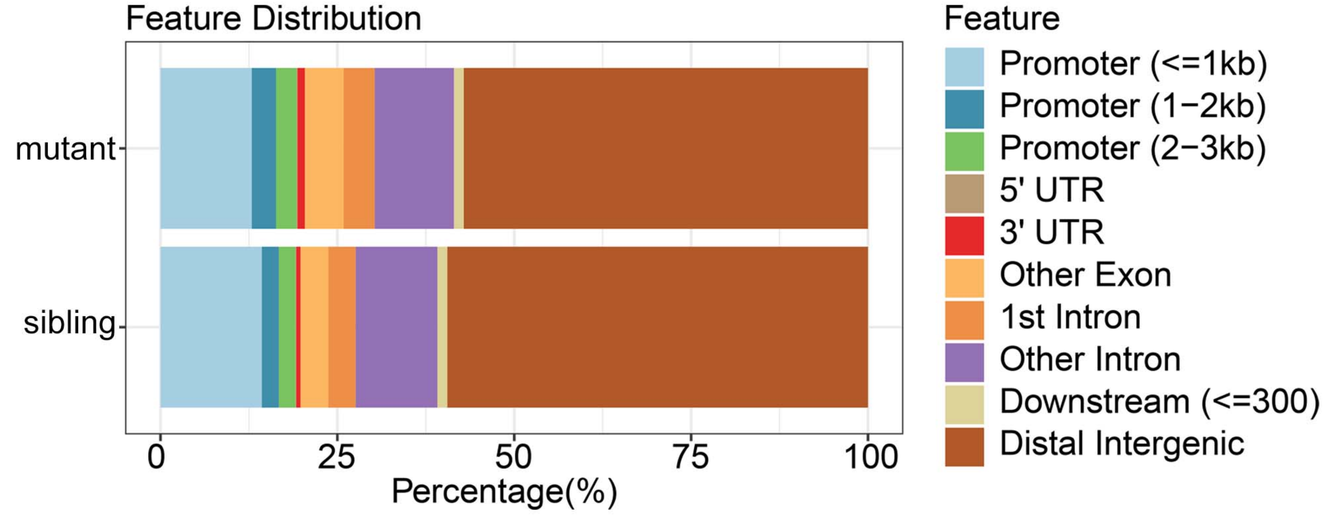

Figure S6

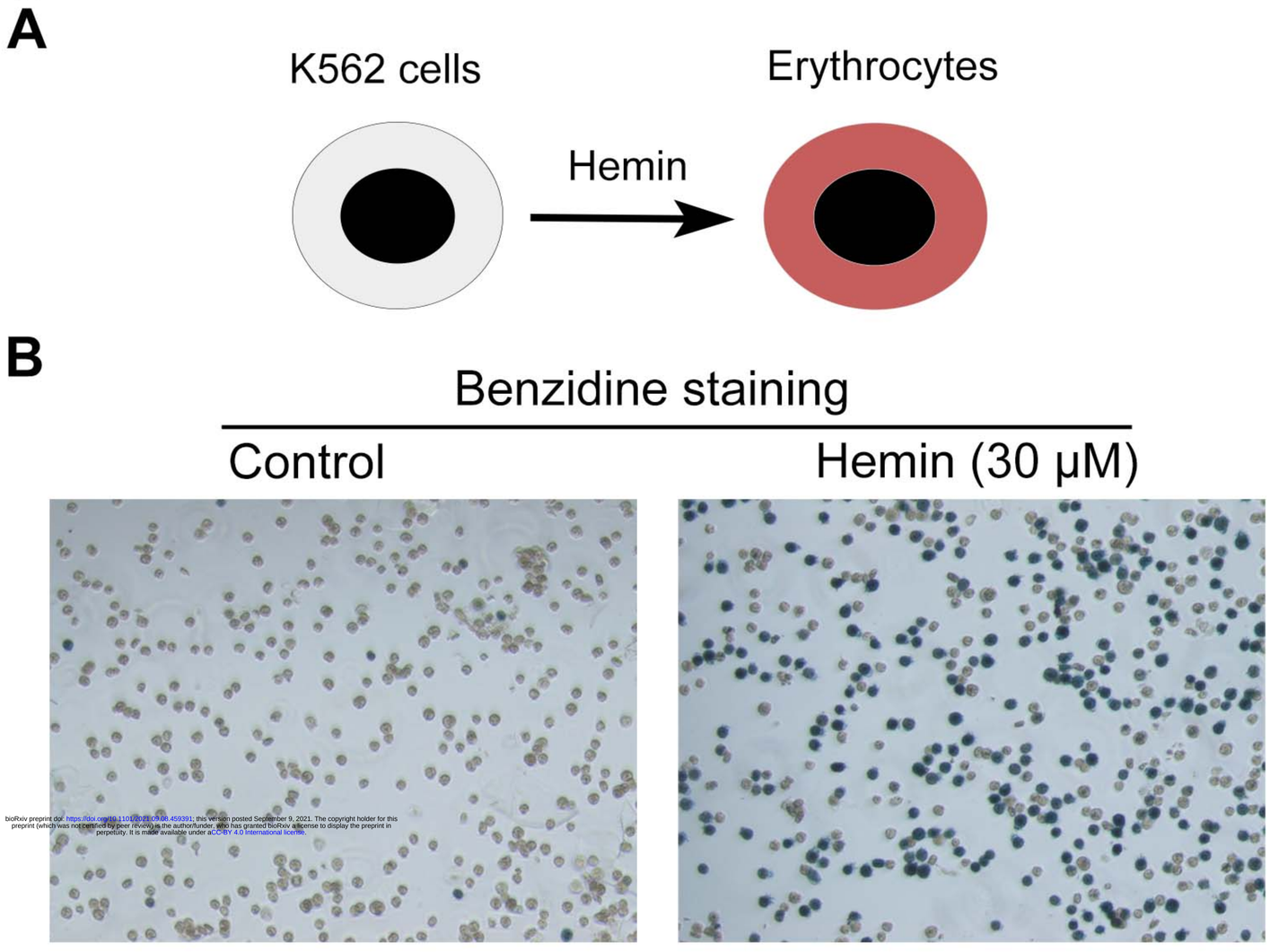

Figure S7

A

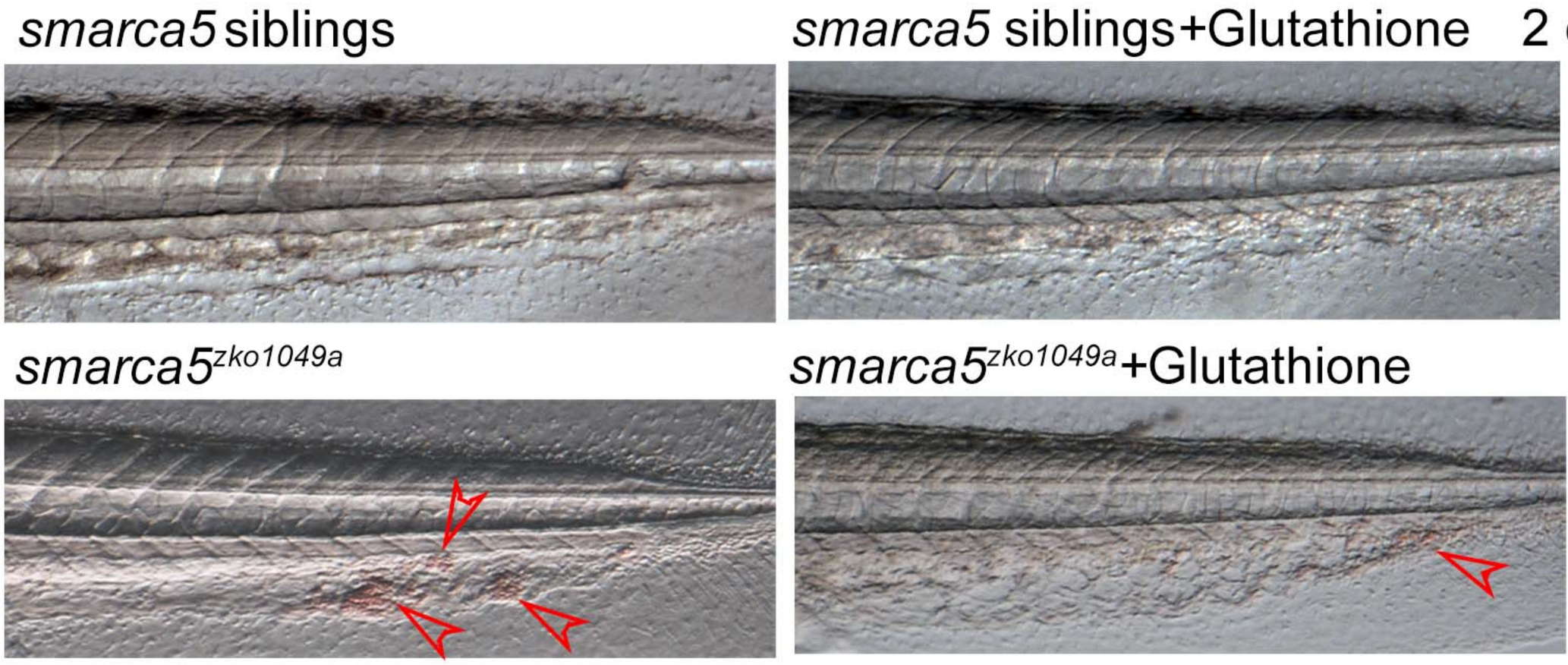

B